Paleogeographic and Morphologic Reconstruction of a Buried Monogenetic Volcanic Field

Alan Bischoff [a]*, Andy Nicol [a], Andrea Barrier [a] and Hanfei Wang [a]

[a] *Department of Geological Sciences, University of Canterbury, Christchurch, New Zealand*

alan.bischoff@canterbury.ac.nz *corresponding author

This is a non-peer reviewed preprint submitted to EarthArXiv.

It has been submitted on February 13, 2019 to Bulletin of Volcanology.

Abstract

Technological advances of our modern society motivated an unprecedented necessity to find natural resources in the subsurface of our planet. The search for these valuable resources has revealed an unexpected number of ancient volcanoes buried and preserved within sedimentary basins globally. Continuous improvements in remote sensing techniques such as seismic reflection can provide a valid opportunity to observe these extinct buried volcanic systems. In this paper, we present the Maahunui Volcanic Field (MVF), a cluster of Miocene volcanoes and shallow intrusions currently buried by more than 1000 m of sedimentary strata of the Canterbury Basin, New Zealand. This 'fossil' volcanic field was imaged by high-quality 2D seismic lines and representative igneous rocks were recovered by the exploration borehole Resolution-1. Here, we present the reconstructed regional paleogeography in which eruptions and shallow (<2 km) intrusions occurred, as well as the original morphology of the volcanoes found in the MVF. Volcanism in the MVF occurred over an area of ca 1,520 km^2, comprising at least 31 crater-and cone-type volcanoes. Eruptions in the MVF typically produced small-volume volcanoes (< 1 km^3), controlled by a plumbing system that fed magma to disperse eruptive centres, a characteristic of monogenetic volcanic fields. The MVF plumbing system emplaced a number of shallow intrusive bodies up to 2.5 km^3 in volume, typically within the Cretaceous-Paleocene sedimentary strata. In many cases, these intrusions have served as a shallow stationary magma chamber that possibly fed eruptions onto the paleo-middle Miocene sea-floor. Eruptions were entirely submarine (500 to 1500 m), producing deep-water morphologies equivalent of maar-diatreme and tuff cones. The morphology of the volcanoes is interpreted to be primarily controlled by high-energy pyroclastic eruptions, in which coeval thermogenic gases and CO_2 incorporated in the magmatic system could have had an important role in the fragmentation and dispersion of erupted material. In addition, post-eruptive degradation has changed the original volcanic morphology, which was controlled by the height of the edifices and by their location in relation to a major base-level fall. By the late Miocene, high volcanic edifices (> 200 m) located in a neritic setting were possibly emergent at the paleo-sea surface, forming an archipelago of nine small extinct volcanic islands. This study demonstrates that despite a number of perceived limitations, the geological history of ancient volcanoes now buried and preserved in sedimentary basins can be reconstructed by detailed seismic stratigraphic mapping and analysis of borehole data.

Keywords: buried volcanoes; monogenetic field; seismic reflection; deep-water eruptions, volcanic plumbing system.

Introduction

Over the last two decades, a growing number of studies have identified the presence of ancient volcanic systems buried and preserved within sedimentary basins (e.g. Field et al. 1989; Herzer 1995; Planke et al. 1995; Planke and Alvestad 1999;

Holford et al. 2012; Schofield et al, 2016; Bischoff et al. 2017). Characterization of these buried volcanoes relies on modern techniques used to observe the Earth's subsurface, such as seismic reflection and borehole drilling (e.g. Planke et al. 2000; Klarner and Klarner 2012; Magee et al. 2013; Penna et al. 2018). However, all remote-sensing and borehole datasets have limitations which place constraints on the resulting interpretations. For example, the quality and resolution of seismic surveys are primarily controlled by geophysical parameters such as signal scattering due to changes in rock velocity and density, energy attenuation with depth, and small geobody thickness relative to the signal wavelength (Abdelmalak et al. 2016; Marfurt 2018). Boreholes can provide valued physical evidences of the subsurface geology, although drilling samples and wireline-logs typically add little information about the geometries and lateral variations within complex three-dimensional rock bodies (Miall, 2000).

To address these limitations, studies of buried volcanoes frequently integrate observations from seismic-scale analogues into the interpretation workflow (e.g. Planke et al. 2017; Gallant et al. 2018; Planke et al. 2018; Bischoff 2019). For example, the morphology of outcropping volcanoes is classically considered to contain valid information of the past eruptive styles, edifice growth mechanisms, and processes of cone degradation experienced during the evolution of a volcanic system (e.g. Cas and Wright 1993; Fornaciai et al 2012; Kereszturi and Németh 2013). However, volcano morphology can be complicated by a number of competing processes including steady vs. dynamic mechanisms of fragmentation, fixed vs. variable locus of explosions, and single vs. multiple eruption phases (Kereszturi and Németh 2013). In addition, morphometric parameters of distinct volcano-types can overlap (Silva and Lindsay 2015), thus, interpreting the past processes that construct and degrade volcanoes based exclusively on their morphology can be problematic. This is especially true for buried volcanoes because, in addition to volcanic complexity and limitations to observe the subsurface geology, the original morphology of these “fossil” volcanoes are likely transformed by superimposed post-eruptive processes such as erosion and compaction (Reynolds et al. 2016; Bischoff 2019).

Despite the perceived difficulties in interpreting volcanoes preserved in the subsurface, seismic reflection interpretation can provide a unique opportunity to observe the complete architecture of buried volcanic systems, combining insights from their plumbing system, morphology of eruptive structures, and impacts of igneous activity on the host sedimentary strata (e.g. McLean et al. 2017; Holford et al. 2017; Bischoff et al. 2019b).

Here, we present the reconstructed morphology and paleogeography of a cluster of Miocene volcanoes currently buried by ca 1000 m of sedimentary strata in the Canterbury Basin, New Zealand’s South Island (Figure 1). We refer to this volcanos to as the Maahunui Volcanic Field (MVF). The name Maahunui is derived from the legendary canoe that the demigod Maui used to sail the Pacific Ocean. In the legend, Maui hooked the great fish Waro, which dragged him for a long distance. When Maui hauled Waro to the surface, the fish transformed himself into land, the North Island of New Zealand, and Maui’s canoe became the South Island. Local Māori people use the name Maahunui for the stretch of coast south of Banks Peninsula (aka Canterbury Bight) and immediately adjacent to the study area. It is notable that modern technology has allowed us to haul rocks of an ancient volcanic field enclosed in the subsurface for more than 10 million years.

MVF was imaged by high-quality 2D seismic lines, with representative igneous rocks collected by the petroleum exploration well Resolution-1 (Figure 1). These datasets have been used to characterize the main eruptive mechanisms that formed some of the volcanoes in the MVF, and to interpret the environments in which intrusions and eruptions occurred in the vicinities of Resolution-1 (Bischoff et al. 2019a). In the present paper, we upscale these interpretations to a regional scale, based on seismic stratigraphic mapping in correlation with data from another five boreholes, and information from outcropping volcanic and sedimentary rocks (Figure 1, 2 and 3). Interpretation of these data has been aided by observations from dozens of outcropping and buried volcanoes imaged by 3D seismic surveys from New Zealand and elsewhere. The datasets are complementary, providing information about the rock-types, eruptive styles, magma-host rocks interactions, volcanic morphologies and volcanic architecture within the Canterbury Basin strata.

Insights from this work help to improve understanding of the processes that control the formation, evolution and preservation of volcanoes now buried in sedimentary basins. The knowledge obtained from the MVF can provide useful insights of how volcanic fields form and evolve elsewhere, including their perceived geological hazards, and potential to contain natural resources.

Geological Setting

Sedimentation in the Canterbury Basin began in the middle Cretaceous (ca 112-105 Ma), synchronous with the rifting event that initiated the separation of Zealandia from west Antarctica and Australia (Laird and Bradshaw 2004; Mortimer et al. 2004). Lithospheric extension created NE-SW and E-W trending grabens in the northern Canterbury Basin, predominately infilled by non-marine late Cretaceous sediments (Sahoo et al. 2015; Strogen et al. 2017; Barrier 2019). Post-rift quiescence and thermal subsidence promoted deposition of marine sequences during the Paleogene, culminating with a maximum transgression during the late Oligocene (Field et al. 1989; Ballance 1993). The present oblique-convergent boundary between the Pacific and Australian tectonic plates has produced tectonic cycles of uplift and erosion in the western border of the basin. These cycles have induced rapid progradation of a thick sequence of continental and marine sediments into the basin since the early Miocene (Suggate et al. 1978; Kamp et al. 1992; Batt et al. 2004; Lu et al. 2005; Figure 1 and 3).

Volcanism occurred semi-continuously throughout the geological evolution of the Canterbury Basin (Field et al. 1989; Barrier et al. 2017; Figure 1). During the Cenozoic, the Canterbury Basin and south-eastern Zealandia experienced widespread and long-lived intraplate volcanism. These magmatic events are not adequately explained by mantle plume or extensive lithosphere thinning models. Two hypotheses have been proposed to explain this atypical magmatic activity: (a) sudden detachment and sinking of a remnant late Cretaceous subducted slab (Finn et al. 2005), and (b) asthenosphere upwelling induced by removal of parts of the subcontinental lithosphere throughout the Cenozoic (Timm et al. 2010). Independent of the geodynamic processes that control this Cenozoic magmatism, the observed products are primarily basaltic in composition, and formed both monogenetic volcanic fields, such as the Waiareka/Deborah and Waipiata Volcanic Fields (Coombs et al. 1986; Németh and White 2003), and large polygenetic volcanic complexes like those of Banks and Otago Peninsulas (Coombs et al. 1960; Sewell 1988).

Scattered large volcanic complexes as well as clusters of smaller volcanoes have been identified buried within offshore strata of the Canterbury Basin since the mid-1970s, with some of the representative igneous rocks penetrated by petroleum exploration wells (e.g. Milne 1975; Field et al. 1989; Blanke 2010; Bischoff 2016; Barrier et al. 2017; Barrier et al. in prep; Figure 1). In the study area, volcanic activity of Miocene age was previously suggested by interpretation of 2D seismic reflection surveys, and by igneous rocks collected by the borehole Resolution-1 (Milne 1975;

Field et al. 1989). Bischoff et al. (2019a) proposed that these seismic anomalies and counterpart igneous rocks are part of a deep-water volcanic field erupted in the northern Canterbury Basin during the middle Miocene. The magmatic products of MVF melts are primarily basaltic-alkaline in composition. Deep-water volcaniclastic rocks of the MVF correlate both in age and in volcanic lithologies with the Wairiri Volcaniclastite, which was erupted in shallow-water and outcrops near Coalgate (Milne 1975; Carlson et al. 1980; Bischoff et al. 2019a; Figure 1).

Dataset, Methods and Limitations

Seismic reflection and well data used in this work were sourced from the 2017 New Zealand Petroleum and Minerals petroleum exploration data pack, which includes a large database of reports, maps, boreholes and seismic surveys loaded into Kingdom© software. We use more than 40,000 km of high-quality 2D seismic lines acquired during the 1970s and 1980s, tied to six boreholes drilled in the northern Canterbury Basin (Leeston-1, Clipper-1, Ealing-1, Resolution-1; Charteris Bay-1 and 2; Figure 1 and 3). Seismic lines typically space <2 km horizontally (maximum of 8 km), with vertical samples recorded at 0.004-second intervals, and depth of imaging up to 6 seconds in penetration (ca 8 km). The borehole datasets vary in quality. Resolution-1 and Clipper-1 contain a more complete set of data that includes lithological, geochemical, geochronological, petrographic and biostratigraphic information from wireline-logs, cuttings and drilling cores (Milne 1975; Hawkes and Mound 1984; Schiøler et al. 2011). Rock-types and interpretations of cuttings and borehole cores from the Resolution-1 well are presented in Bischoff et al. (2019a).

Combining seismic reflection interpretation and borehole analysis, we mapped ten regional chronostratigraphic surfaces from the late Cretaceous to the modern seabed, along with two important unconformities from the early and late Miocene (Figure 1, 2 and 3). The mapping follows sequence stratigraphic principles such stratal reflection relationship and depositional trends within seismic facies (e.g. Mitchum et al. 1977; Hunt and Tucker 1992; Catuneanu et al. 2010). In addition, we have undertaken a seismic volcano-stratigraphic analysis of the study area (Planke et al. 1999) by mapping the lateral continuity of the pre-eruptive surface (PrErS) and post-eruptive surface (PoErS) of the MVF, tied to the first and last occurrence of middle Miocene extrusive rocks identified in Resolution-1 (Bischoff et al. 2019a; Figure 2 and 3). Additional stratigraphic analysis of the study area includes mapping of the post-degradational surface (PoDgS) and the post-burial surface (PoBuS), according to the method proposed in Bischoff (2019). These stratigraphic surfaces bind stages of degradation and burial of the MVF edifices after volcanic activity has ceased in the field. They correspond to the time in which the burial rate exceed the erosion rate in the MVF (PoDgS), and when the presence of the buried volcanoes of the MVF no longer impact sedimentation in the study area (PoBuS).

Seismic facies analysis was conducted for all anomalies that could represent middle Miocene igneous bodies buried in the northern Canterbury Basin. This characterization is based on criteria such as geometry, internal and external configuration of seismic reflectors, deformation of enclosing strata, and stratigraphic position of the anomaly in relation to the mapped chronostratigraphic surfaces (Mitchum et al. 1977).

Detailed morphologic characterization was undertaken for each seismic anomaly that is considered to possibly correspond to a middle Miocene volcano of the MVF (Figure 4 and 5; Appendix 1). To reconstruct the original morphometric parameters of volcanoes now buried in the subsurface, three key parameters have to be addressed: i) the acoustic velocity of the material within and enclosing the igneous seismic anomalies, ii) the amount of post-eruptive degradation of the volcanoes before burial, and iii) how much compaction the volcanoes experienced during their burial, from the the time of their formation at the surface to their actual depth in the basin. Table 1 shows the parameters, assumptions, and limitations necessary to characterize and reconstruct buried volcanoes.

Initially, we classify the post-burial morphology of potential volcanoes in the MVF (i.e. as the volcanoes appear on seismic lines) according to their geometry as cone-and crater-type morphologies (Figure 4 and 5). Next, we divide the cone-type morphologies into four classes: positive symmetric cone, positive asymmetric cone, positive trapezium and positive mound. Crater-type morphologies were divided into 2 classes: funnel-and basin-shaped geometries. Basal width (W) of cone-type volcanoes was measured by the horizontal distance between the inflection points of the PoErS horizon in relation to the PrErS horizon (Figure 4a). The width of crater-type volcanoes corresponds to the horizontal distance between the edges of their craters at the PrErS level (Figure 4b).

The edifice height and depth of craters was initially recorded as two-way-time (TWT) in seconds (Figure 4a and b). To convert this TWT measurement to an acceptable distance in meters, we evaluate the apparent acoustic impedance of volcanic seismic facies in contrast to seismic facies that correspond to the enclosing Tokama Siltstone. The acoustic velocity of this siltstone averaged around 2700 m/s, which is recorded in sonic wire-line logs of the Resolution-1 borehole. Thus, volcanic seismic facies with similar impedance contrast compared to enclosing siltstones were assigned a velocity of 2700 m/s, while seismic facies showing stronger and weaker acoustic signals were assigned as 3000 m/s, and 2500 m/s respectively.

To estimate post-eruptive degradation of MVF volcanoes, we mapped seismic features that could indicate those parts of the edifices that were eroded and remobilized. These features include volcanoes that display flattened tops concordant with the stratigraphic position of major base-level-falls, and the presence of localized seismic facies that may indicate debris material deposited next to the edifice flanks. In all cases of inferred edifice degradation, we have estimated the amount of erosion by measuring the distance between the top of the eroded edifice (PoErs), and the intersection of lines projected along the volcano flank towards its estimated original summit (Figure 5). Thus, the amount of degradation was classified as low (< 20 m vertically), moderate (20 to 100 m), high (> 100 m), or "unsure" in cases where the volcanic seismic facies showed poor seismic resolution.

To estimate the amount of compaction experienced by the volcanoes in the MVF, we assess seismic features that could indicate differential compaction between the buried volcanoes in contrast to the surrounding Tokama Siltstone. Compaction curves for sediments in the Canterbury Basin indicate that siltstones buried at 1000 m (average burial depth of the MVF), typically have compacted around 30% relative to silt at the surface (Field et al. 1989). Volcanoes showing a domed configuration of overlying reflectors indicate that enclosing siltstones compacted more than the MVF volcanic rocks during progressive burial (e.g. Planke et al 2005; Bischoff et al. 2017; Holford et al. 2017). Flat reflectors overlying volcanoes indicate no differential compaction, while reflectors showing a 'seagull wing-shaped' configuration suggest that the enclosing Tokama Siltstone was compacted less than the volcano. Thus, we assign 20% compaction for volcanic seismic facies showing burial doming, 30% when displaying flat overlying reflectors, and 40% when associated with "seagull wing" configuration (Figure 4 and 5).

With the available dataset (Appendix 1), we reconstruct a proxy original morphology of the MVF volcanoes. Table 2 shows the equations applied to calculate the morphometric parameters of these ancient volcanoes. Further information of the method applied to reconstruct the morphology of the MVF is detailed in Bischoff (2019).

Paleogeography of the MVF

Pre-eruptive stage (prior to 12.7 Ma)

During the early Miocene and prior to the onset of volcanism in the MVF at 12.7 Ma (Bischoff et al. 2019a), seismic stratigraphic mapping shows that sedimentation in the northern Canterbury Basin was controlled by a low-gradient ramp aligned with the Chatham and Endeavour structural highs (Field et al. 1989; Barrier 2019; Figure 3 and 6). This smooth ramp has a concave geometry gently dipping towards the regional basin depocenter in the SE (Figure 6d). At the location of Resolution-1, biostratigraphic data presented in Schiøler et al. (2011) indicates a deep-lower bathyal setting (1500 to 2000 m) during the Altonian (18.7 to 15.9 Ma). This paleoenvironmental condition changed to lower bathyal (1000 1500 m) at ca 15 Ma, which occurs in association with a major base-level fall and development of an early Miocene unconformity in the study area (Table 3; Figure 2).

Integration of the results from borehole data, seismic stratigraphic analysis and information from paleogeographic maps presented in Field et al. (1989) and Sahoo et al. (2015) indicates that the pre-eruptive bathymetry of the study area ranges from lower bathyal at its shallowest, to deep-lower bathyal at its deepest segment (Figure 6d).

Syn-eruptive stage (12.7 to 11.5 Ma)

During the syn-eruptive stage of the MVF, a deep-water setting remained relatively stable in the study area (Bischoff et al. 2019a; Figure 6; Table 3). Lower bathyal conditions (1000 to 1500 m water depths) favour the deposition of fine-grained sedimentary rocks of the middle Tokama Siltstone unit until ca 11 Ma (Bischoff et al. 2019a; Figure 2), which is evident in biostratigraphic data of the Resolution-1 well (Schiøler et al. 2011). The middle Tokama Siltstone depositional unit is locally interbedded with volcaniclastic rocks comprising abundant glassy shards, relics of bubble walls, spheroidal fragments enveloped in a palagonite film (possible armoured lapilli), broken phenocrysts, and lithics, indicating that eruptions near the location of Resolution-1 occurred in a deep-submarine environment (Milne 1975; Bischoff et al. 2019a).

The chronostratigraphic map of 11.5 Ma shows that the paleo-seafloor morphology of the study area drastically changed from a smooth ramp (Figure 6d) to a hilly ramp (Figure 6c) after volcanic activity in the MVF. Results from seismic stratigraphic analysis indicate that this morphological modification is associated with a rise of the paleo-seafloor above shallow intrusive bodies (< 1 km), and the addition of cone-type volcanoes onto the middle Miocene paleo-seafloor (Figure 3 and 4c and d).

Isochron maps of the interval from 15.9 to 11 Ma indicate that a thick pile of rocks was deposited in association with the edifices of the MVF (Figure 7b). Accumulation of material within these volcanoes formed a localized bathymetric high in the northern Canterbury Basin during the middle Miocene (MVF submarine high; Figure 6c and 7b). Seismic stratigraphic mapping indicates that initial stages of construction of a pronounced shelf-break morphology is associated with the location of the MVF volcanoes. In the area surrounding the MVF, this prominent basin-slope morphology initiates to form during the middle to late Miocene, which is not observed in other parts of the basin until the early Pliocene (Lu et al. 2003; Figure 3, 5 and 8a).

During its active stage all volcanoes in the MVF appear to be located in a lower bathyal environment, however, some shallower bathymetries are expected to have been present at the location of volcanic edifices and above large intrusions (Figure 4; Figure 6c).

Post-eruptive stage (11.5 to 11 Ma)

After volcanism ceased around 11.5 Ma (Bischoff et al. 2019a), the MVF was progressively buried by an increase in sediment influx from the NW, which is interpreted to be derived from the early uplift events that built the New Zealand Southern Alps (Field et al., 1989). Chronostratigraphic and isochron maps show that the presence of the extinct submarine volcanic edifices had a local influence on the distribution of sediments in the area (Figure 6 and 7b). Seismic imagery displays a distinctive low-gradient setting occurring among cone-type edifices of the MVF, which is interpreted as a low-energy sedimentary environment in Bischoff (2019b).

By 11 Ma, most volcanoes in the MVF were completely buried in a lower to uppermost bathyal setting, with the exception of the pc14 and pc09, as both of these volcanoes were partially buried and located in deeper waters (Figure 6b). After 11 Ma, the remaining deep-water cone-type volcanoes pc09 and pc14 were buried by the progressive NW-SE basin-slope progradation, which occurred simultaneously with the establishment of Banks Peninsula in the late Miocene (Figure 3, 6 and 7).

Igneous Seismic Facies

We describe six distinctive igneous seismic facies in the study area: (1) crater-type, (2) cone-type, (3) saucer high-amplitude, (4) disrupted, (5) tabular sub-vertical, and (6) horizontal high-amplitude (Figure 8). Table 4 shows the main characteristics of these seismic facies.

Crater-type seismic facies (Figure 8b) are characterized by funnel-and basin-shaped geometries that penetrate into the PrErS horizon. Internal reflectors within this negative seismic facies are moderate-amplitude, chaotic, and disrupted at its lower part, which gradually becomes sub-parallel and continuous towards the upper part. External reflectors below the PrErS horizon are parallel and semi-continuous. Immediately above the PrErS, a set of symmetric high-amplitude reflectors occur laterally to both sides of the central part of the funnel-shaped craters (Figure 8a and b). The amplitude of these symmetrical reflectors decreases in intensity as the distance from the crater increases (Figure 8a). In magma-rich sedimentary basins, crater-type seismic facies usually are interpreted as negative buried volcanic and/or hydrothermal vents (e.g. Planke et al. 2005; Alvarenga et al. 2016; Oliveira et al, 2018), showing morphological equivalence to those classified as crater dominated-type volcanoes in the Earth’s surface (Kereszturi and Németh 2013).

Cone-type seismic facies are characterized by convex upward projections between the PrErS and PoErS horizons, forming morphologies such as mounds, trapeziums and cone-shaped structures (Figure 8). The central part of cone-type seismic facies typically displays disrupted, chaotic, and inward-dipping internal reflections, which laterally grade to semi-continuous and outward-dipping sub-horizontal reflectors (Figure 8c). These lateral reflectors occur as stacked sets on both sides of the central cone-shaped structures, showing downlap terminations onto the PrErS horizon distal to its central part. In sedimentary basins affected by magmatism, cone-type seismic facies are typically interpreted as positive buried volcanic vents (e.g. Holford et al. 2012;

Reynolds et al. 2016; Barrier et al. in prep.), such as those classified as cone dominate-type volcanoes by Kereszturi and Németh (2013).

Saucer high-amplitude seismic facies typically show a single high-amplitude reflector with saucer-shaped morphology. In cross-sectional view, this seismic facies presents a sub-horizontal inner sheet parallel to the enclosing strata, and two peripheral inclined sheets cross-cutting adjacent strata (Figure 8d). This seismic facies is commonly interpreted to correspond to igneous intrusions emplaced into sedimentary rocks. These saucer-bodies occur in great numbers in the Canterbury Basin (Blanke 2010; Barrier et al. 2017), and are described in the literature as saucer-shaped sills (e.g. Hansen and Cartwright 2006; Holford et al. 2012; Gallant et al. 2018), although their contact with enclosing strata typically shows both sill and dike relationships.

Disrupted seismic facies are zones in which continuous, parallel and horizontal basinal reflectors are displaced in simple and complex patterns, and/or are offseted by intruding cross-cutting reflectors (Figure 8e). The upper part of disrupted seismic facies usually shows reflectors in a dome geometry, while its lower part is commonly associated with loss of seismic reflectivity, typically displaying chaotic aspect and reflectors in a cross-cutting relationship (e.g. Jackson 2012; Schofield et al. 2016; McLean et al. 2017). Disrupted seismic facies are interpreted to indicate brittle deformation of host strata due to emplacement of intrusive bodies (e.g. Infante-Paez and Marfurt 2017; Bischoff et al. 2017; Angkasa et al. 2017).

Tabular sub-vertical seismic facies correspond to steeply inclined, moderate-to high-amplitude reflectors with tabular geometry (Figure 8f). This sub-vertical seismic facies typically occurs below the top basement horizon of the Canterbury Basin, in alignment with pre-Cretaceous fault structures and in a cross-cutting relationship with the basement fabric. However, this seismic facies also occurs in shallower levels, cross-cutting sedimentary sequences. Spatially, this seismic facies can occur as a single inclined reflector, or in association with saucer-shaped high-amplitude, disrupted seismic facies, and also below crater-and-cone type seismic facies. Tabular seismic facies as those described in the MVF are typically interpreted as dikes and magmatic conduits cross-cutting host rocks elsewhere (Infante-Paez and Marfurt 2017; Bischoff et al. 2017, Morley 2018).

Horizontal high-amplitude seismic facies show tabular geometry and have a parallel relationship with the basin strata (Figure 8g). These horizontal reflectors differ from the seismic expression of typical basin strata because of the the strong high-amplitude contrast with adjacent layers, commonly occurring in association with underlying disrupted seismic facies. Horizontal high-amplitude seismic facies indicate the emplacement of large sill intrusions parallel with the host sedimentary strata (Schofield et al. 2012; Gallant et al. 2018), commonly displaying the highest impedance peaks in seismic imagery of the study area.

Volcano Morphology Reconstruction

We reconstruct the proxy morphology of 31 crater-and cone-type seismic features that could represent ancient volcanoes of middle Miocene age buried in the northern Canterbury Basin. The constraints applied to characterize each of these volcanoes are shown in Appendix 1.

Results of the post-burial morphological analysis (i.e. as the volcanoes appear in seismic lines) show that 81% of the volcanoes in the MVF have a cone-type morphology, most of which are positive cones (42%). Volcanoes that excavate into the PrErS horizon (crater-type) comprise only 19% of the MVF (Figure 9a). The width (W) of the MVF volcanoes ranges from 550 to 6350 m. Most volcanoes (71%) have a W between 1000 and 3000 m (Figure 9b). The anomalous volcano with W > 6000 m was interpreted from a low confidence seismic anomaly, and may correspond to a cluster of highly eroded amalgamated volcanoes, rather than a single edifice.

Results from estimation of the magnitude of degradation of the cone-type volcanoes (Figure 9c) shows that most edifices experienced low (erosion has removed < 20 vertical meters) to moderate degradation (20 to 100 m), while seven volcanoes were probably highly eroded (>100 m). It was not possible to determine the magnitude of degradation for five volcanoes due to poor seismic quality. Most crater-type volcanoes (84%) have overlying domed reflectors or show no evidence of differential compaction relative to the enclosing Tokama Siltstone. This result suggests that the majority of crater-type volcanoes have compacted ca 20 to 30 % from their original post-eruptive form (9d).

The reconstructed volcanic morphology indicates that the original edifice heights of the MVF volcanoes varied from around 60 to 430 m, while original slopes ranged from 5° to 24° (Figure 9e and f; Appendix 1). Cone-type volcanoes mostly range in original height from 100 to 300 m, with only 16% of the volcanoes falling outside of this range. Original slope angles of cone-type volcanoes typically are low-angle, with 84% of the data ranging from 5° to 15.9°. The original volume calculated for cone-type volcanoes show results varying from 0.0057 to 3.2610 km^3, in which 83% of the edifices are <1 km^3 (Figure 9h). The total depth of crater-type volcanoes vary from 90 to 230 m (Figure 9g). Three of these craters have overlying small cone-type volcanoes.

Contrasting the results of the reconstructed morphology vs. the paleogeographic position of the volcanoes in the MVF suggests that at 11 Ma (post-eruptive stage), cone-type edifices higher than 200 m and located proximal to the shelf-break experience intense degradation when compared with cone-type edifices located in deep-waters (Figure 10).

Plumbing System and Eruptive Vent Distribution

Seismic reflection interpretation revealed that the MVF plumbing system emplaced a number of intrusive bodies into the sedimentary strata of the northern Canterbury Basin (seismic facies d to g in Figure 8). The upper part of the MVF plumbing system is characterised by a network of shallow intrusions (< 3 km), comprising individual and swarms of sills, dikes, saucer-sills, and stocks (Bischoff et al. 2019b). The emplacement of these intrusions produced intense deformation of the host basin strata, forming complex arrays of faults and folds that tilted and disrupted layers of pre-magmatic sequences (Figure 4, 5 and 8).

Large intrusions typically display a saucer-shaped geometry (Figure 11), in which the most expressive bodies are ca 25 km^2 in area, and have an estimated thickness of approximately 100 m, considering the acoustic velocity recorded for the monzogabbro intrusion penetrated by Resolution-1 (ca 5000 m/s; Milne, 1975). This suggests that individual saucer-intrusions could have volumes as great as 2.5 km^3. In this work, we did not calculate the total volume of magma crystalized within the shallow MVF plumbing system due to a perceived limitation to characterize the 3D geometry of complex igneous intrusions using 2D seismic reflection datasets. However, the great number of intrusive bodies observed in the seismic data of the study area suggests that the total volume of all of the shallow intrusions of the MVF could be greater than 50 km^3.

Seismic mapping of eruptive vents and their associated seismically detected volcanic apron indicates that volcanism in the MVF covers an area of ca 1,520 km^2. These volcanoes typically erupted at individual locations (Figure 1 and 12), forming a cluster of crater-and cone-type small-volume volcanoes. Together, cone-type volcanic edifices have an estimated volume around 20 km^3, excluding any erupted material that may have drifted in the water column or was deposited as thin ash layers (< 1m) interbedded with the Tokama Siltstone (Appendix 1). Comparing results from the intrusive and extrusive parts of the MVF, it is likely that a greater volume of magma has been emplaced within the basin sedimentary strata, while a smaller volume would have reached the surface.

In many cases, we observe a relationship between the location of large intrusive bodies and overlying cone-and crater-type volcanoes, which is evident by an array of faults and fractures that connect these intrusions to the root of eruptive vents (Figure 4, 11 and 13). Most volcanoes (68%) are likely related to these large and shallow saucer-shaped intrusions, suggesting that these igneous bodies could have fed eruptions in the MVF (Appendix 1 and 2). In addition, Bischoff et al. (2019a) observed a petrogenetic relationship between the middle Miocene intrusive and extrusive rocks perforated by the borehole Resolution-1.

The constrained observations indicate that the MVF plumbing system comprised numerous isolated and/or interconnected shallow magma batches that have possibly served as stationary magma chambers for eruptions onto the middle Miocene paleo-seafloor. However, a deeper (>5 km from the limits of our dataset) source-to-surface plumbing system is also likely to have fed some of the volcanoes in the MVF (Bischoff et al. 2019b; Appendix 2). Clusters of small-volume volcanoes controlled by a plumbing system that feeds magma to disperse eruptive centres are characteristic of monogenetic volcanic fields (e.g. Cas and Wright 1993; Németh 2010; Kereszturi and Németh 2013; Silva and Lindsay 2015; Németh and Kereszturi 2015).

Controls on Volcano Morphology

Volcano morphology can provide important insights of processes such as past eruptive styles and edifice growth mechanisms experienced during the evolution of volcanoes (e.g. Dohrenwend et al. 1986; Takada 1994; Tibaldi 1995; Vesperman and

Schmincke 2000; Martin and Németh 2006; Corazzato and Tibaldi 2006; Valentine et al. 2007; apud Fornaciai et al. 2012). Integration of the results from morphological and paleogeographic reconstruction of the study area allows us to understand that two main processes controlled the morphology of the MVF volcanoes: i) eruptive-style, which produced distinguishable cone-and crater-type morphologies, and ii) differential degradation of cone-type volcanoes, which is a consequence of volcanic edifices been exposed to different paleoenvironmental conditions.

Eruptive Styles and Volcanic Growth Mechanisms

Crater-type volcanoes

Combining the results of seismic morphological reconstruction and information from volcaniclastic rocks of the Resolution-1 borehole (Bischoff et al. 2019a) suggests that MVF crater-type volcanoes experienced some form of intense material fragmentation and dispersion, as is typically accredited with the formation of maar-diatreme volcanoes (e.g. Kereszturi and Németh 2013; Silva and Lindsay 2015; White and Valentine 2016; Figure 13a). The 2D seismic morphology of this volcano-type shows a large inward-dipping and steep central crater. Both sides of the crater display low angle (ca 5º) outward-dipping flanks that extend up to 5 km in width (Figure 13a).

The structure of the central crater varies from unbedded and chaotic in the lower part, to bedded and sub-horizontal in the upper part, as observed in maar-diatreme volcanoes elsewhere (Lorenz 1985; White and Ross 2011; Figure 4b). The formation of these craters is likely related to processes such as brittle deformation, mass collapse and adjustment of pre-eruptive material into large depressions created by high-energy pyroclastic eruptions (Kereszturi and Németh 2013). Deep excavations into pre-eruptive host rocks requires significant energy and intense material fragmentation (Zimanowski et al. 1997; White and Valentine 2016). The interpretation of high-energy pyroclastic eruptions is also supported by the large symmetrical flanks of the crater-type volcanoes, which possibly indicate widespread dispersion of erupted material and deposition at a low angle of repose next to the crater zone (Figure 8a and b).

Cone-type volcanoes

Results from the reconstructed morphology of the MVF cone-type volcanoes indicate that this volcano-type was constructed by accumulation of layers of tephra near to a vent zone. The seismic morphology of cone-type volcanoes is dominated by a set of reflectors superimposed onto and above the pre-eruptive horizon. These staked reflectors form a convex-upward seismic facies, in which the PoErS horizon is projected above a relatively flat PrErS horizon, becoming parallel to basinal layers with increasing distance from the centre of the structure (Figure 4a and 5).

This geometric relationship indicates that material was sourced from a central location, which we interpret to correspond to the eruptive centre of crater-type volcanoes (Figure 8a and c). The interpretation of a central vent is supported by reflectors dipping inward towards the centre of the structure, while peripheral reflectors are outward-dipping and downlap onto the PrErS horizon. These peripheral outward-dipping reflectors are interpreted to correspond to the flanks of crater-type volcanoes (Figure 13b). In addition, the central part of cone-type volcanoes often displays a relationship with underlying intrusive bodies (Figure 8 and 15).

The structure of the conduit zone shows minor excavations into the pre-eruptive horizon, which indicates that mechanisms of fragmentation and dispersion of erupted material had less energy that the processes that formed the crater-type volcanoes (White and Valentine 2016). Below the MVF cone-type volcanoes, disrupted pre-eruptive strata with layers upward-dipping are commonly observed, which likely indicates processes of magmatic deformation at sub-volcanic level (Figure 4). We consider that seismic artefacts such as pull-up of velocities (Jackson 2012; Magee et al. 2013) have little effect on the configuration of reflectors below the MVF volcanic vents. Typically, the reflector configuration of the sub-volcanic zones of the MVF do not show a direct geometric relationship with the overlying vent. In counterpart, sub-volcanic zones of MVF cone-type volcanoes typically show structural patterns coherent with the position of underlying intrusive bodies, and have a spatial relationship with seismic facies that indicate the presence of magmatic conduits, faults and fractures (Figure 5, 8, 13b and 15). Magmatic deformation of host sedimentary strata are commonly reported to occur beneath volcanic edifices (Planke et al. 2005, Bischoff et al. 2017; McLean et al. 2017; Morley 2018; Gallant et al. 2018).

The flanks of cone-type volcanoes show abrupt topographic inflections above the vent zone, with average reconstructed slope angles <16° (Figure 4a and 9f). The width of these flanks typically extend < 2 km from the vent. These are common morphometric ranges of outcropping tuff cones (Kereszturi and Németh 2013; Silva and Lindsay 2015), and indicate that ejected tephra material accumulates nearly to the vent zone, when compared with crater-type volcanoes (Figure 13). In addition, representative MVF rocks from Resolution-1 contain fine-grained particles with broken crystals, possible armored lapilli and ash aggregates (Bischoff et al. 2019a), which are typical textures of deposits formed by eruption-fed density currents (White 2000).

The reconstructed paleogeography of the MVF indicates that cone-type volcanoes formed in water-depths ranging from a minimum of 500 m to a maximum of 1500 m depth (Figure 12). This suggests that cone-type volcanoes likely erupted entirely submarine, seeing that the highest edifice located at shallower waters has an original height estimate of 420 m. Although our dataset indicates entirely submarine volcanism in the MVF, we cannot discard that minor subaerial or Surtseyan eruptions have occurred, mainly from volcanoes located in an ultra-proximal setting. This is also true for volcanoes not imaged on our seismic dataset.

Cone-type volcanoes of the MVF can include deep-water equivalent of tuff cones and maybe spatter cones. Tuff cones are typical products of phreatomagmatic eruptions (Kereszturi and Németh 2013; Silva and Lindsay 2015), in which ballistics comprised of blocks and bombs and turbulent jets represent the main mechanisms of particle dispersal (Cas et al. 1989; Kaulfuss et al. 2012). Spatter cones are usually the products of lava fountaining, commonly formed during Hawaiian and Strombolian type eruptions (Kereszturi and Németh 2013; Silva and Lindsay 2015). These volcano-types have been reported in both subaerial and subaqueous environments (e.g. Deardoff et al. 2011; White et al. 2015a; White et al. 2015b; Cas and Giordano 2014).

In the MVF, the shallow slope angle (<16º) of the flanks cone-type volcanoes suggests that they may correspond to tuff cones, however, the seismic expression of tuff and spatter cones may be difficult to distinguish based on morphometric parameters. Thus, we do not discard the occurrence of spatter cones in the MVF. Pillow-mounds are also possible to have formed in the MVF, however our dataset indicates that cone-type volcanoes are more likely formed by the accumulation of tephra material rather than superimposed layers of lava deposits. Mound and trapezium-shaped seismic anomalies are interpreted to represent progressive degradation of original cone-shaped volcanoes (Figure 5 and 15), as a result of exposure of the cone crest to wave erosion during the lM unconformity, discussed in the next section.

Post-Eruptive Degradation

After the MVF eruptions ceased around 11.5 Ma, seismic stratigraphic and biostratigraphic analysis indicate a progressive shallowing in water depths. This event occurs simultaneously with the wake of the basin-slope progradation from NW to SE in the northern Canterbury Basin. By ca 11 Ma, the MVF can be divided into two halves by the position of a proto-shelf break (Figure 12). The shallower NW part was located in an outer neritic environment (<100-200 m), while the deeper SE was set in an uppermost to mid bathyal setting (>200-1000 m). Volcanoes with original heights >200 m and located proximal to the 11 Ma proto-shelf break show increasing amounts of degradation (e.g. flattened-tops relative with the lM unconformity, reflectors downlaping from the edifice into basin strata), while volcanoes located distal to the proto shelf-break were buried and well preserved independent of their original post-eruptive height (Figure 5 and 14). In addition, volcanoes classified to have had a low amount of degradation show a cone morphology in both shallow and deep-water settings, while highly degraded volcanoes are always located proximal to the 11 Ma shelf-break position (Figure 10; Appendix 1). This differential degradation suggests that the top of volcanoes located at shallower waters may have been removed by erosion.

Clague et al. (2000a) demonstrates that flat-topped volcanoes in Hawaii can form as continuously overflowing lava ponds, even in deep-water environments. This situation is unlikely to explain the flattened-tops of the MVF cone-type volcanoes because the accumulation of lava deposits typically displays high-amplitude reflectors in seismic imagery (e.g. Planke et al. 1999; Holford et al. 2012; Reynolds et al. 2017). The MVF volcanoes do not show tops with high-amplitude reflectors, with the exception of the volcano pm02 (Figure 5). In addition, the volcanoes with flattened-tops in the MVF always have their upper part associated with the position of the lM unconformity (Figure 5 and 15). We interpret that some originally high (>200 m) cone-type volcanoes located at shallower waters at 11 Ma may have emerged above sea-level. In this case, these emergent volcanoes have likely experienced degradation of their tops by wave erosion, and may have formed an archipelago of at least nine small volcanic islands by ca 11 Ma (Figure 12).

Discussion

The MVF shows random vent distribution of cone and crater-type volcanoes in relation to water-depth (Figure 12). Magma decompression and fragmentation in deep-water settings are still mechanisms not completely understood (e.g. White et al. 2015a; Cas and Giordano 2014; Cas and Simmons 2018). Observations from the Kermadec Island Arc indicate a transition from explosive to effusive volcanism around 1000 m (Wright et al. 2006), however, products of explosive eruptions have been inferred to also occur in deeper settings elsewhere (e.g. Clague et al. 2000a; Planke et al. 2005; Head and Wilson 2003; White et al. 2003).

Zimanowski and Büttner (2003) argue that subaqueous volcanic thermohydraulic explosions become increasingly improbable at water depths >100 m, and practically impossible in settings deeper than 1000 m. However, Clague et al. (2000a) inferred that phreatomagmatic activity occurred at a depth of ca 1300 m at the Loihi seamount, offshore Hawaii, which is approximately equivalent to the depth of the root zone of the volcanoes studied here. Cas and Simmons (2018) point out that subaqueous effusive eruptions can produce fallout deposits of ash-size autoclastic vitric material similar to typical deposits of subaqueous pyroclastic eruptions. This autoclastic process could explain the textures of the volcaniclastic rocks recovered in the Resolution-1 without necessarily requiring a large explosive process. However, autoclastic mechanisms of fragmentation cannot explain the large craters excavated into the PrErS horizon, nor the seismic facies that suggests high-energy mechanisms of fragmentation and dispersion of material (e.g. Lorenz 1985; White 2000; Kereszturi and Németh 2013; White and Valentine 2016).

The reconstructed paleogeography of the MVF allows us to confidently interpret that crater-type volcanoes were erupted at waters depths around 1000 m (Figure 12). It is notable that most of the volcanoes in the MVF show a relationship with large intrusive bodies emplaced into organic-rich host rocks. In addition, the high content of coal lithics and limestones found in the volcaniclastic rocks representative of the MVF (Bischoff et al., 2019a) could indicate that CO_2 and CH_4 were incorporated into the magmatic system (Aarnes et al. 2015). These gases may have contributed additional energy to overcome the hydrostatic pressure typically imposed in deep-water settings, as proposed by Sversen et al. (2004) and Agirrezabala et al. (2017). In normal conditions, it would be expected that the elevated hydrostatic pressure will supress the development of large pyroclastic eruptions (Zimanowski and Büttner 2003).

The constraining dataset indicates that crater-and cone-type seismic morphologies were mainly formed by large deep-water pyroclastic eruptions. However, some volcanoes in the MVF could have experienced different dominant eruptive mechanisms rather than high-energy eruptions. Possible eruptive-types of the MVF could also include phreatic activity in the absence of magma (Planke et al. 2005), or subaqueous processes similar to those observed in Strombolian and Vulcanian eruptions, which can form the submarine equivalent of spatter cones (e.g. Deardoff et al. 2011; White et al. 2015a; Cas and Giordano 2014).

The crucial challenge of modern deep-water volcanology is the need to improve understanding of how diverse mechanisms of fragmentation, dispersal and deposition of volcanic material are not affected by changes in the hydrostatic pressure alone. Factors such as deformability vs. compressibility and the critical point of the water, thermal conductivity, incorporation of CH_4 and CO_2 into the magmatic system, and the degree of induration of the country rock are dynamic forces that together with hydrostatic pressure play an important role in the final style of subaqueous eruptions (e.g. Sversen et al. 2004; Kereszturi and Németh 2013; White et al. 2015a and b; Cas and Giordano 2014; Agirrezabala et al. 2017; Cas and Simmons 2018).

Conclusions

Volcanism in the Maahunui Volcanic Field (MVF) occurred over an area of ca 1,520 km^2, comprising of a cluster of at least 31 middle Miocene volcanoes. These volcanoes are currently buried by approximately 1000 m of sedimentary strata in the offshore part of the northern Canterbury Basin. Seismic reflection interpretation coupled with information from borehole data allow us to reconstruct the proxy paleogeography of the study area, and to estimate the original morphology of the volcanoes of the MVF. Volcanic edifices typically had a small-volume (<1 km^3) immediately after their eruptive phase. MVF eruptions were short-lived and controlled by a plumbing system that fed magma to dispersed eruptive centers, a characteristic observed in monogenetic volcanic fields. The MVF plumbing system emplaced a number of shallow (<1000 m depth) intrusive bodies, commonly within Cretaceous-Paleocene sedimentary strata. Saucer-shaped sills are the typical intrusion-style, presenting estimated volumes of up to 2.5 km^3. These shallow intrusions likely fed magma to some, if not most, of the MVF volcanoes. It is estimated that a greater volume of magma has been emplaced within the basin sedimentary strata, than magma that was likely erupted. Eruptions were entirely submarine (500 to 1500 m), most likely producing subaqueous equivalents of maar-diatreme and tuff cone volcanoes. The morphology of the MVF volcanoes is interpreted to be primarily controlled by high-energy pyroclastic eruptions in which incorporation of coeval thermogenic gas and CO_2 into the magmatic system likely have an important role in the fragmentation and dispersion of ejected material. In addition, post-eruptive degradation has changed the original volcanic morphology, which was influenced by the height and the position of the volcanic edifices in relation to a late Miocene base-level fall. After volcanism ceased, volcanoes located in a bathyal setting were rapidly buried and preserved, while volcanoes located in a neritic setting and with edifice heights >200 m were likely emergent at the paleo sea-surface. By the late Miocene, these emerged volcanoes have possibly formed an archipelago with at least nine small extinct volcanic islands. This study demonstrates that perceived limitations to interpret the geological history of ancient volcanoes now buried and preserved in sedimentary basins can be overcome by detailed seismic stratigraphic mapping and analysis of borehole data. Insights from this work can help to improve understanding of the processes that control the formation, evolution and preservation of these buried volcanoes. The knowledge obtained from the ancient volcanoes of the MVF can contribute to the understanding of how volcanic fields form and evolve elsewhere, including their perceived geological hazards, and their potential to contain natural resources such hydrocarbons, groundwater, metals and geothermal energy.

Table 1: Attributes and parameters used to characterize the seismic morphology, and to reconstruct the volcanoes in the MVF. See Appendix 1 for details.

Seismic morphometric parameters	Shape of the anomaly after burial, basal diameter (m), height after burial (s) for cone-shaped anomalies, depth after burial (s) for crater-shaped anomalies.
Assumptions and estimations	Post-eruptive degradation, burial compaction and acoustic velocity of the volcanic seismic facies. Edifice volume calculation approximated to the volume of a cone.
Other considerations	Seismic data quality, position of the 2D seismic line relative to the centre of the seismic anomaly, evidence for large intrusions underlying anomalies, paleo-geographic position relative to major base-level falls, seismic facies that suggest reworking of the volcanic anomaly.

Table 2: Equations used to calculate seismic morphometric parameters of the MVF volcanoes.

Abbreviations	Equations
HaBs: height after burial in seconds **Vel:** estimated acoustic velocity in m/s **HaBm:** height after burial in meters **comp:** estimated amount of compaction (%) **HbBm:** height before burial in meters **degr:** estimated amount of degradation in meters **oHm:** estimated original eruptive height in meters **W:** basal width in meters **Rt:** basal radius in meters **HW:** height vs. basal width ratio **oS:** estimated eruptive flank slope in degrees **atan:** arc cotangent **oV:** estimated edifice original volume in km^3 **π:** 3.141592	$HaBm = \frac{HaBs \times Vel}{2}$ $HbBm = HaBm + (HaBm \times comp)$ $oHm = HbBm + degr$ $HW = \frac{oHm}{W}$ $oS = 180^0 \times \frac{\text{atan}(oHm/Rt)}{\pi}$ $oV = \pi r^2 \, (oHm/3)$

Table 3: Main stratigraphic and paleoenvironmental characteristics of the MVF area. Interval highlighted in red corresponds to the active eruptive time in the volcanic field.

Age	Regional Morphology	Magmatic stage	Depositional setting	Shallower waters (NW)	Deeper waters (SE)
11 Ma and younger	Slope-and-basin	Complete	Neritic to uppermost bathyal	100 to 200 m and progressively shallower	200 to 400 m and progressively shallower
Post-degradational surface (unconformity IM) and rapid progradation					
11.5 to 11 Ma	Onset of slope-and-basin in the MVF area	Degradational	Uppermost bathyal to mid bathyal	200 to 400 m (volcanoes ≥ 200 m were emerged above sea-level)	600 to 1000 m (≥ 100 m at volcano summits)
Post-eruptive surface and onset of progradation					
12.7 to 11.5 Ma	Ramp, hilly at the MVF location	Syn-eruptive	Lower bathyal	500 to 750 m (≥ 80 m at volcano summits)	1000 to 1500 m (≥ 200 m at volcano summits)
Pre-eruptive surface					
Early Miocene and priory to 12.7	Smooth ramp	Pre-eruptive	Lower to deep bathyal	1000 to 1500 m	1500 to 2000 m

Table 4: Main aspects of the middle Miocene igneous seismic facies of the study area.

Seismic facies	Geometry	External	Internal	Below	Above	Strat. location	Interpret.
Crater-type	Funnel-and basin-shaped	Semi-continuous and parallel	Chaotic, offset and parallel	Offset, saucer-shaped, loss of reflection	Flat, domed	Into PrErS	Crater-type volcanoes
Cone-type	Cone, mound and trapezium-shaped	Oblique, continuous and parallel	Chaotic, inward-and outward dipping	Offset, saucer-shaped, loss of reflection	Domed, onlap	Above PrErS and below PoErS	Cone-type volcanoes
Saucer high-amp	Saucer-shaped	Parallel, cross-cut	High-amp, continuous to offset	Offset, complex	Flat, domed, offset	Cretace. Paleocene	Saucer-shaped intrusions
Disrupted	Complex	Parallel, offset, cross-cut	High-amp to loss of reflection	Offset, loss of reflection	Domed, offset	Within all seismic facies	Bridged host strata and dikes
Tabular sub-vertical	Tabular inclined	Cross-cut	Single of group of cross-cutting reflectors	Offset, loss of reflection	Domed, flat	Basement and below vents	Dikes and magmatic conduits
Horizontal high-amp	Tabular sub-horizontal	Parallel	High-amp continuous	Offset, loss of reflection	Domed, flat	Cretace. to Miocene	Large sill intrusions

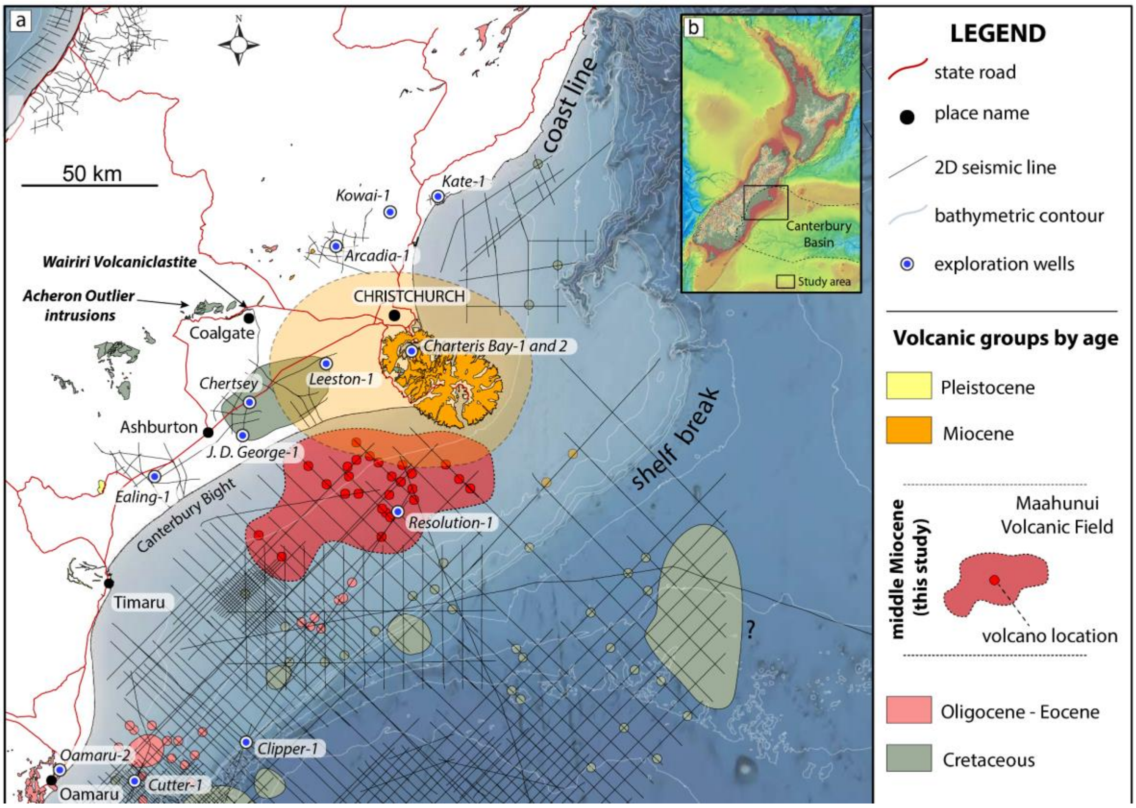

Figure 1: (a) Map showing the age and location of volcanic rocks onshore and offshore of the northern Canterbury Basin, together with the main seismic and well data used in this work. Onshore volcanic rocks are from Forsyth et al. (2008). Red dots indicate the location of volcanoes in the MVF. (b) New Zealand topographic and bathymetric map from the NZ Petroleum Exploration 2018 datapack. Black square in (b) shows the location of the detailed map in (a).

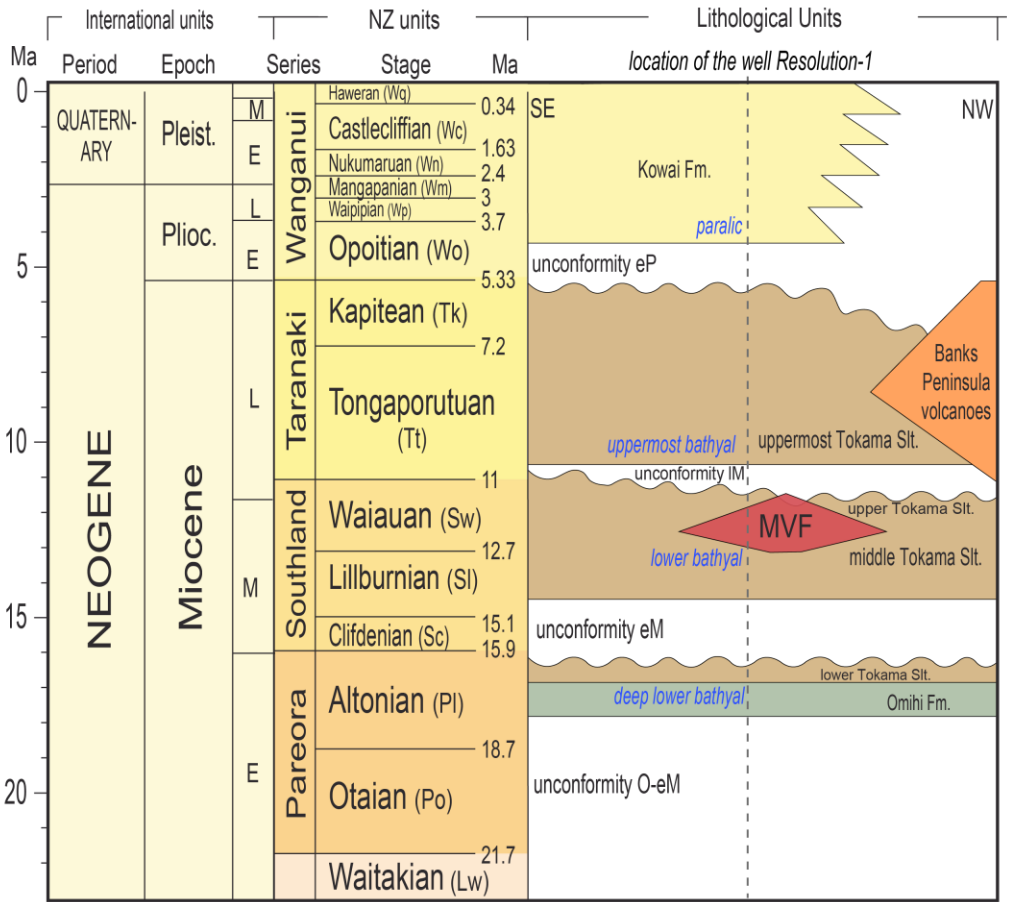

Figure 2: Local chronostratigraphic chart of the study area with emphases on the extrusive part of the MVF. Stratigraphic ages follow the International Chronostratigraphic Chart 2014 and the New Zealand Geological Time Scale 2015 (Raine et al. 2015). See Bischoff et al. 2019a for characterization of the Tokama Siltstone depositional units (lower to uppermost).

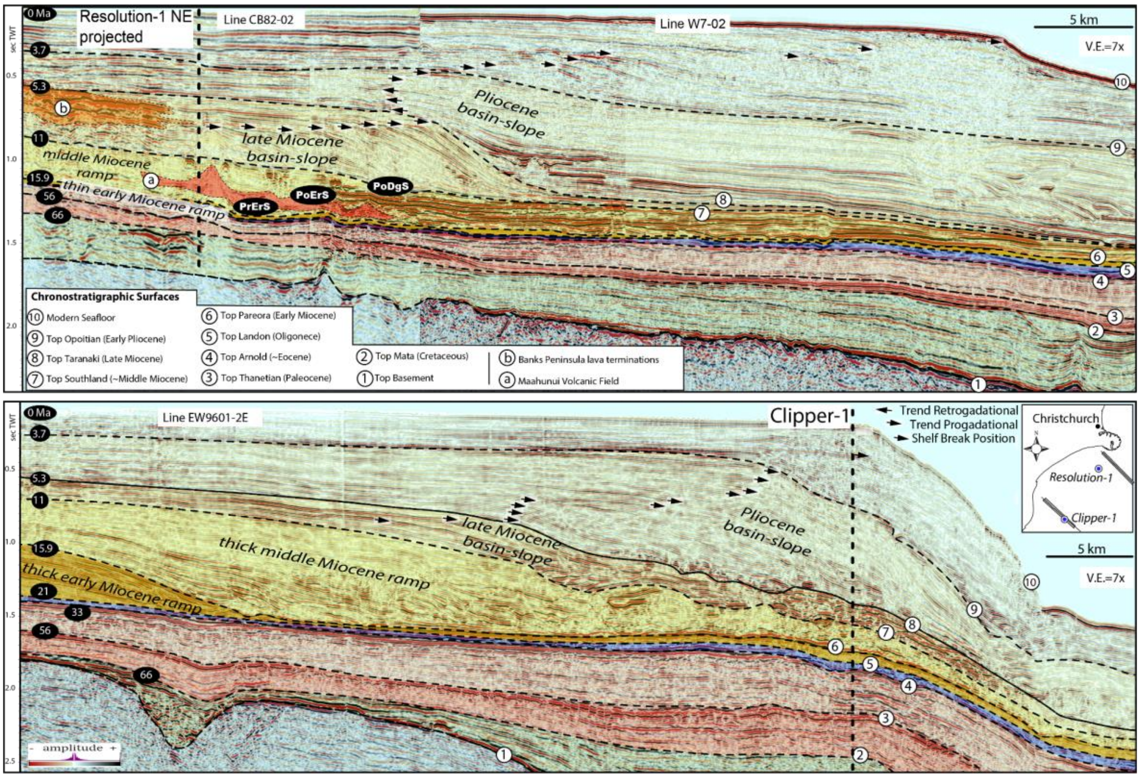

Figure 3: 2D seismic lines showing the offshore basin architecture of the northern Canterbury Basin from Cretaceous to recent, and the location of MVF. Arrows show the position of the shelf-break during the latest Neogene, with the arrowhead pointing in the direction of progradational and retrogradational depositional trends. Abbreviations are: pre-eruptive surface (PrErS), post-eruptive surface (PoErS) and post-gradational surface (PoDgS).

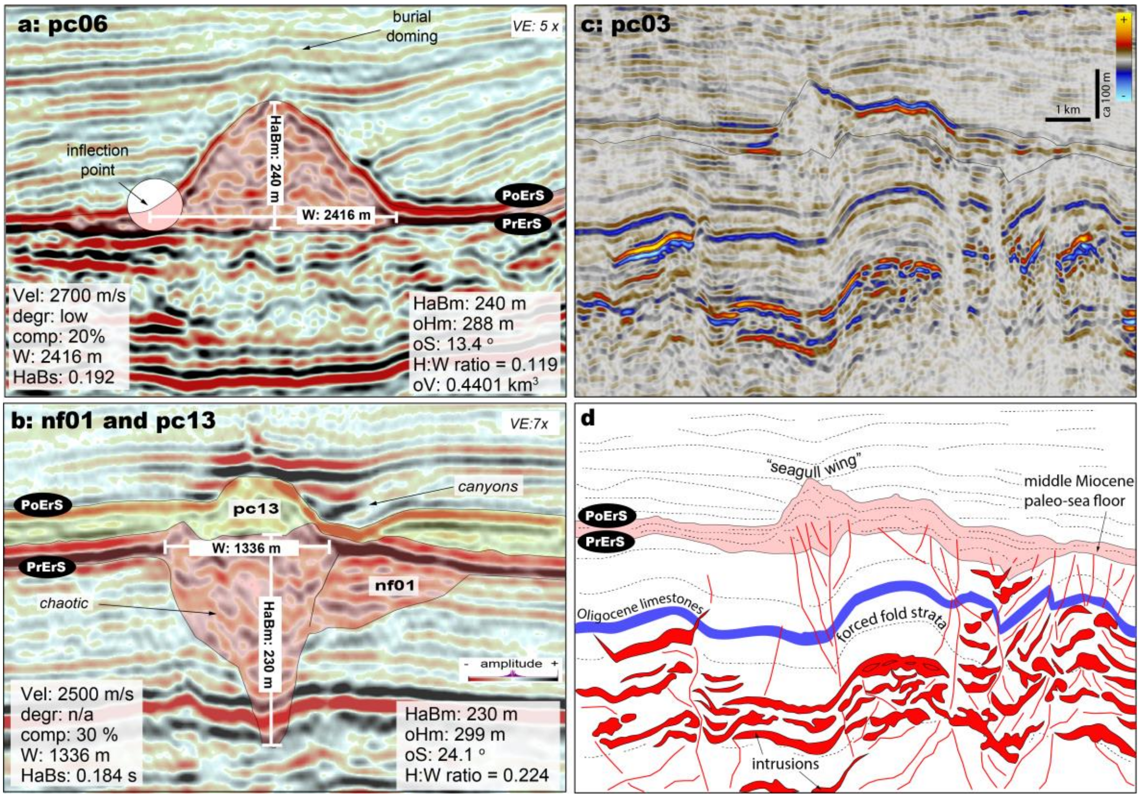

Figure 4. Examples of volcanoes of the MVF. (a) shows the morphology of a positive symmetric cone (cone-type). (b) shows a compound morphology. The bottom part (nf01 in light red) has a negative funnel-shaped geometry (crater-type) and shows the lateral seismic facies association. The upper part (pc13 in light yellow) shows a positive asymmetric cone shape (cone-type) and its lateral seismic facies association. Data in the white squares refer to morphometric parameters of pc06 (a) and nf01 (b). Abbreviations are shown in Table 2. (c and d) uninterpreted and interpreted 2D seismic image of the volcano pc03 and part of the MVF shallow plumbing system. Note the deformed pre-eruptive strata above intrusions.

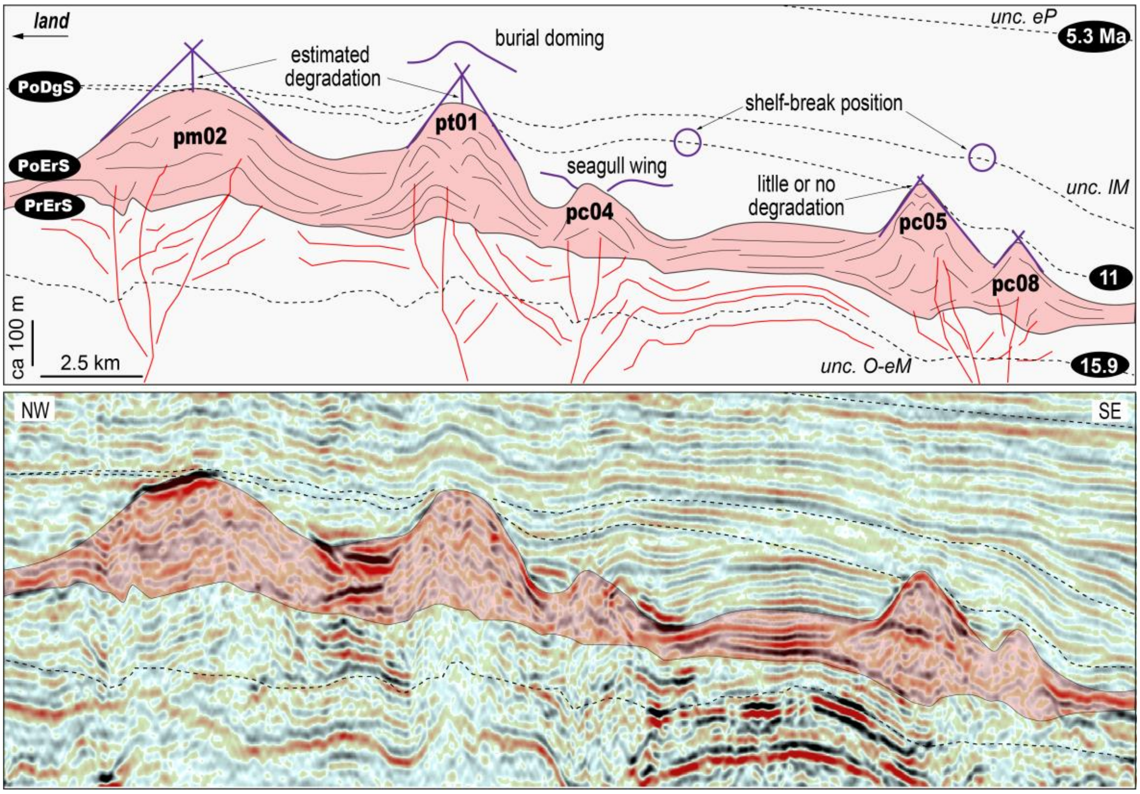

Figure 5: 2D dip section (line CB-82-06) showing the morphology of some of the volcanoes in the MVF. Note a progressive degradation from the volcano pc08 to pm02, relative with the development of a late Miocene (lM) unconformity. Morphometric parameters of these volcanoes are shown in Appendix 1.

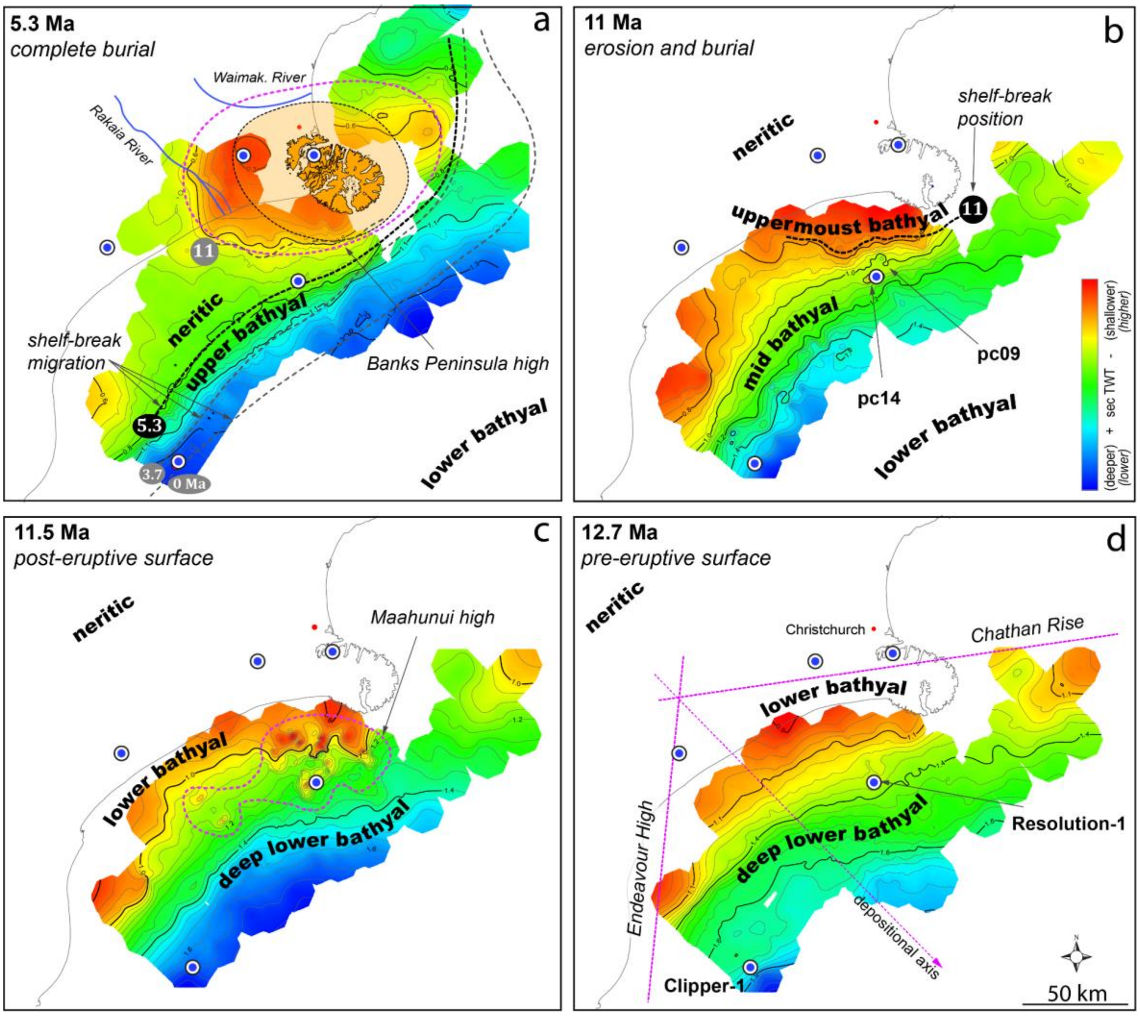

Figure 6: Neogene chronostratigraphic maps of the study area. During the Miocene, the paleogeography of the northern Canterbury Basin evolved from a smooth ramp (d) to a basin-slope morphology (a). MVF erupted entirely in a lower bathyal setting during the middle Miocene (d and c). The addition of these volcanic edifices onto the paleo-sea floor of the northern Canterbury Basin has formed a localized elevated topography (shown as Maahunui high in c). The volcanic field was buried during the late Miocene in a lower to uppermost bathyal setting due to rapid SE sediment progradation (b and a). Inland paleoenvironments compiled from Field et al. (1989).

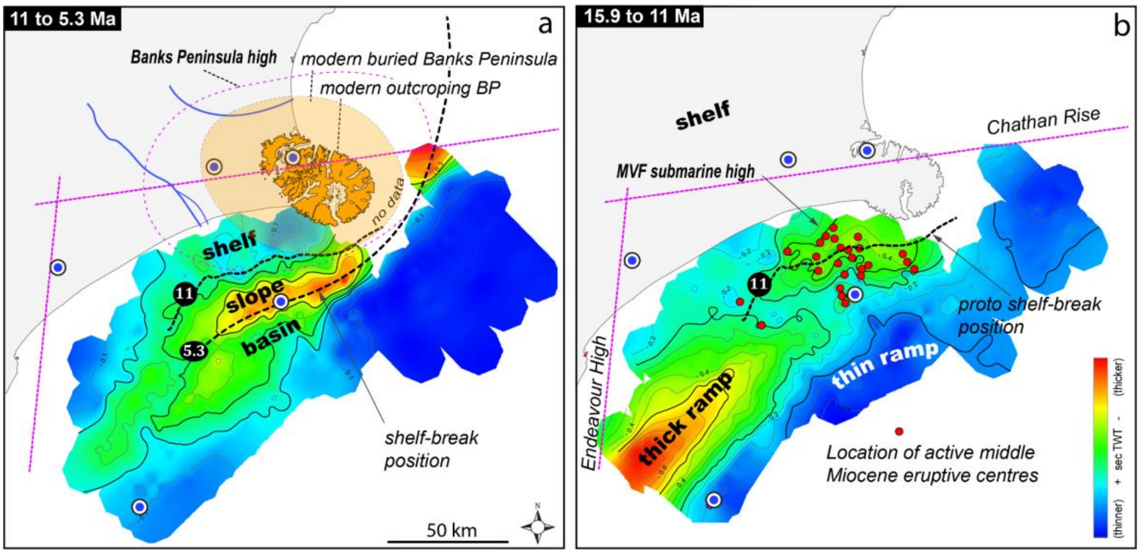

Figure 7: Neogene isochron maps of the northern Canterbury Basin. Note in (b) that a thick pile of sediments were deposited within the MVF edifices. The isochron map in (b) includes pre-magmatic strata from 15.9 Ma and post-eruptive strata up to 11 Ma. By the late Miocene (after 11 Ma), most volcanoes were buried by the slope progradation associated with increasing sediment supply from the NW, simultaneously with the emplacement and eruptions of the Banks Peninsula (a).

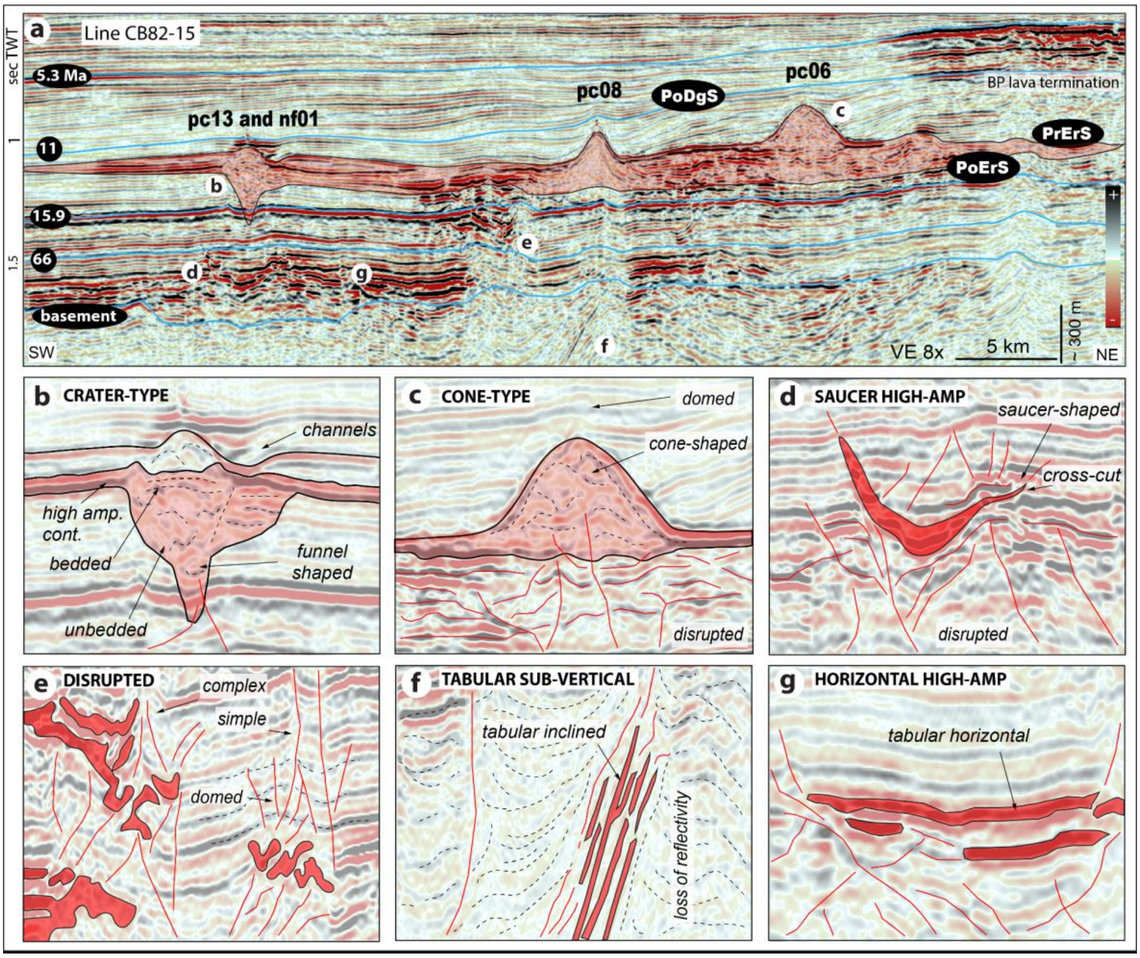

Figure 8: Igneous seismic facies of the study area. (a) Regional 2D strike/oblique seismic line showing the lower (PrErS) and upper (PoErS) stratigraphic limits of the MVF and the location of representative igneous seismic facies. (b and c) show volcanic (extrusive) seismic facies, while figures (d to g) show images of parts of the MVF plumbing system. Morphometric parameters of these volcanoes are presented in Appendix 1. High-amplitude reflectors in the upper right corner of (a) are interpreted as the termination of lava flows deposits of the Banks Peninsula volcanoes.

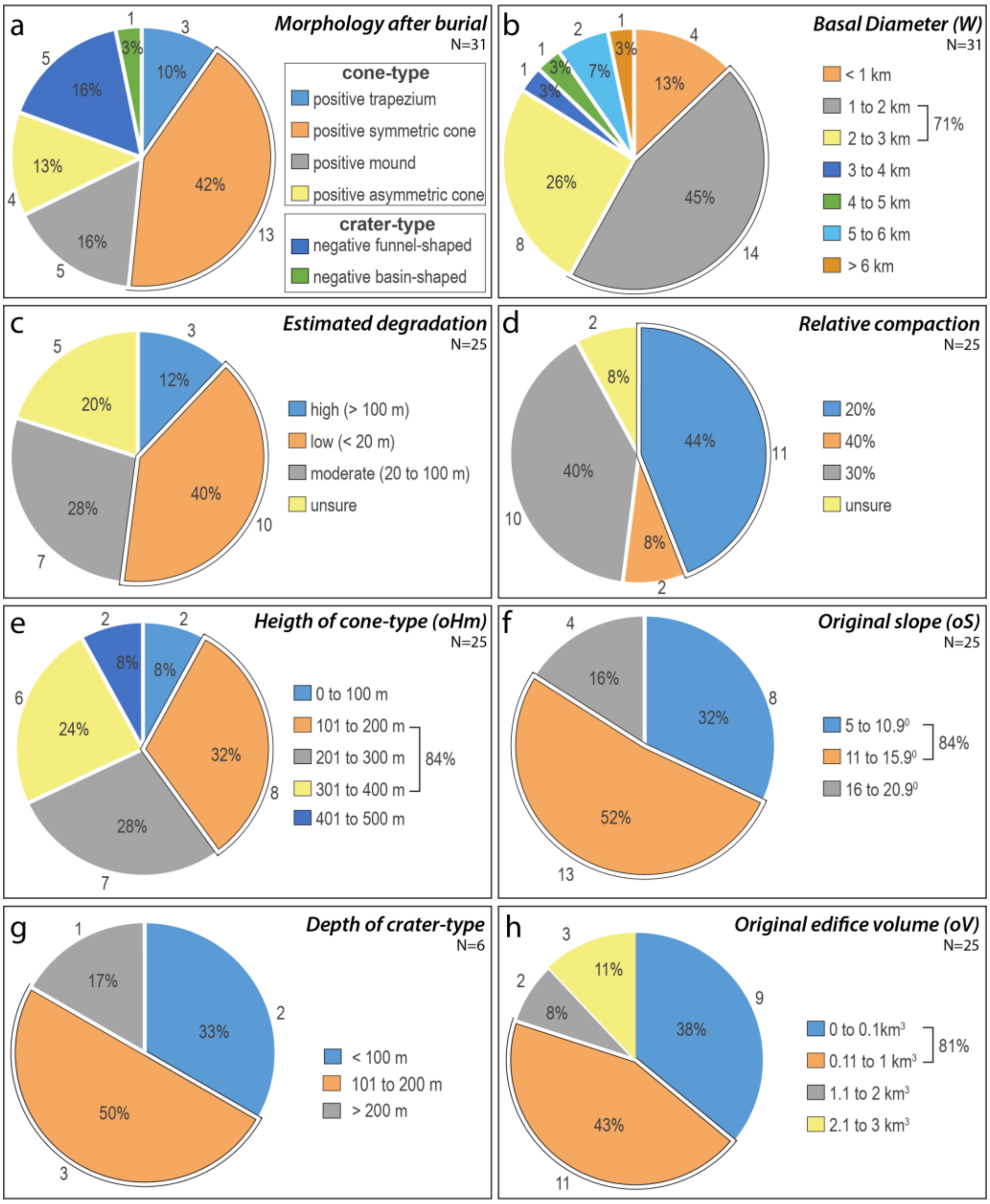

Figure 9: Diagrams showing the morphometric results from the volcanoes of the MVF. See text for details.

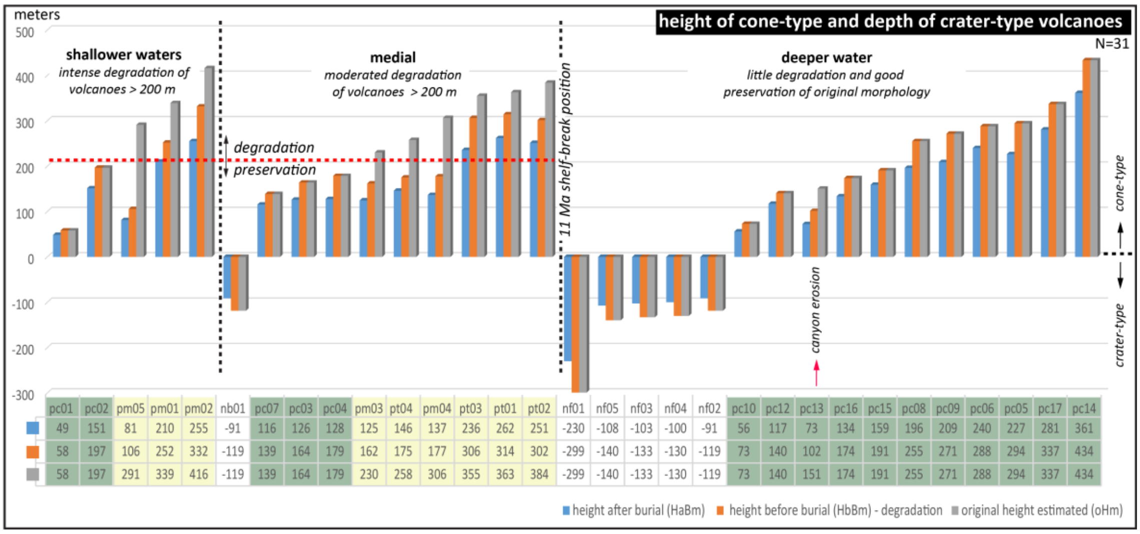

Figure 10: Morphometric analysis of MVF volcanoes relative to their post-eruptive paleoenvironmental location (ca 11 Ma). Blue bars show the height of volcanoes after burial (HaBm). Orange bars show values of the decompacted volcanic heights (HbBm). Grey bars show values of the reconstructed original height of the MVF volcanoes (oHm). Red dashed line shows the interpreted limit between preservation and degradation of the MVF cone-type volcanoes (e.g. pm03 vs. pc04). Numbers highlighted in green are cone-shaped morphologies. Numbers highlighted in yellow are mounds-and trapezium-shaped morphologies, and in white are crater-type volcanoes. The red arrow points to the only pc volcano located in deeper waters at 11 Ma which shows evidence of being eroded by canyons.

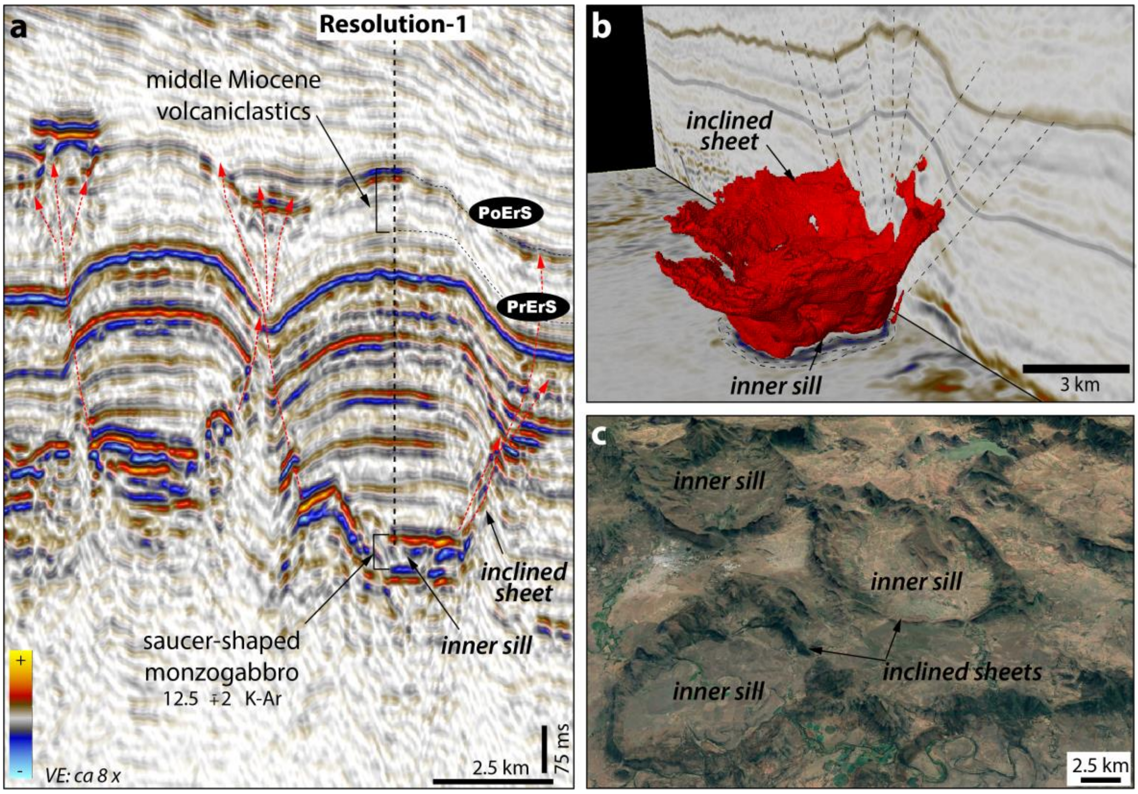

Figure 11: (a) seismic line at the location of the borehole Resolution-1 showing a saucer-shaped sill in 2D section. Red dashed lines indicate potential pathways for magma and hydrothermal fluids to migrate up-sequence. Vertical scale is shown in milliseconds (ms). (b) example of 3D visualization of a saucer-shaped sill emplaced in sedimentary strata of the Taranaki Basin, North Island of New Zealand. The 3D morphology of this intrusion was mapped by extracting the seismic amplitude of an area of interest (red). (c) Google Earth image of saucer-shaped sills outcropping in the Karoo Basin, South Africa (Gallant et al. 2018). Note the dominant morphology of the saucer-sills that show an inner sill morphology, and a ring of peripheral inclined sheets. See Bischoff et al. (2019a) for complete petrographic characterization of the igneous rock-types of the Resoltuion-1.

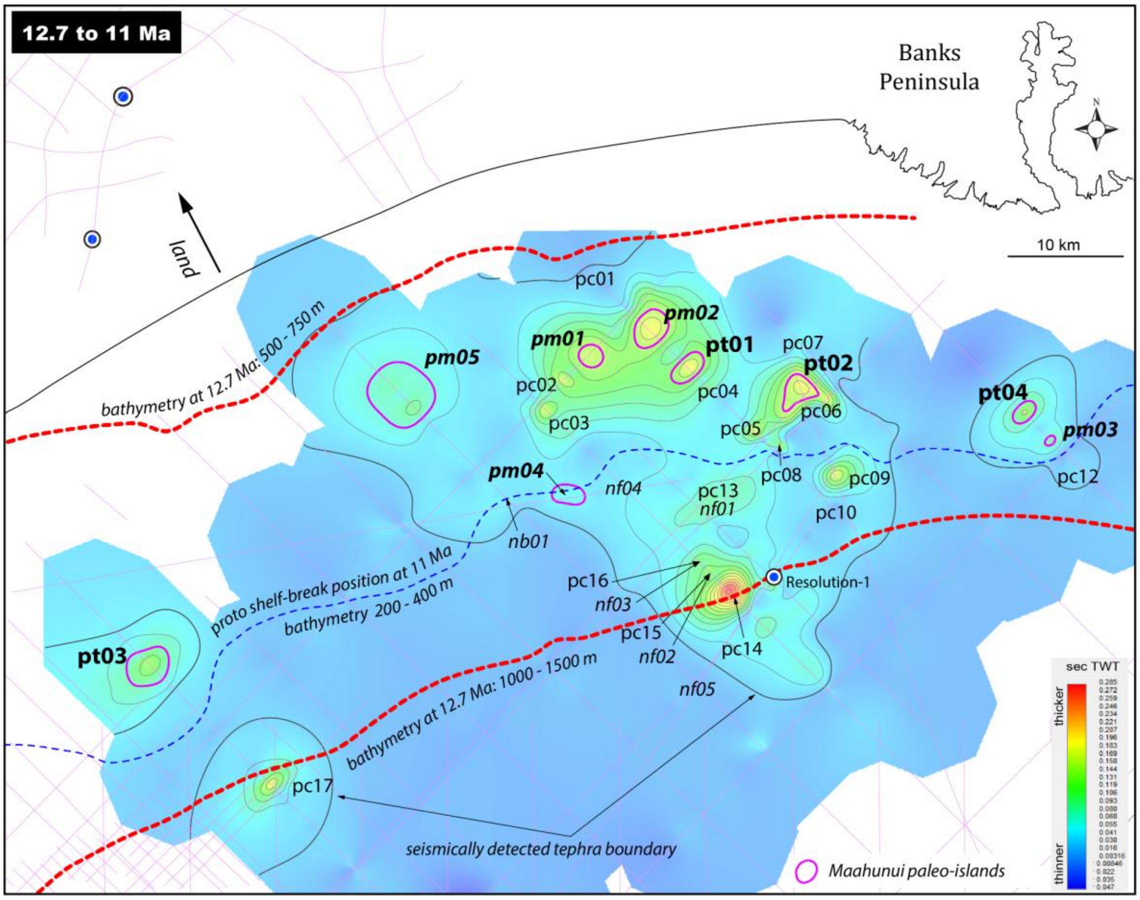

Figure 12: Composite paleogeographic and paleoenvironmental map of the study area from 12.7 to 11 Ma. Abbreviations correspond to their morphology and are plotted at the location of the volcanoes. Pc's are positive cones, pt's are positive trapezium, pm's are positive mounds, nf's are negative funnel-shaped structures and nb's are negative basin-shaped seismic anomalies. Red dashed lines show the approximate bathymetry at the onset of eruptions in the MVF. Blue dashed line shows the position of ta proto-shelf-break at 11 Ma. Note that all pm's and pt's are located within relatively shallower waters, proximal the 11 Ma shelf-break. Volcanoes distal to the 11 Ma proto-shelf break show a sharp increase in slope towards their summit, while volcanoes located proximal to this line show shallower slopes, which suggest a progressive degradation of cone-shaped to mound-shaped morphologies. Volcanoes highlighted in purple possibly correspond to an ancient archipelago comprising nine small extinct volcanic islands.

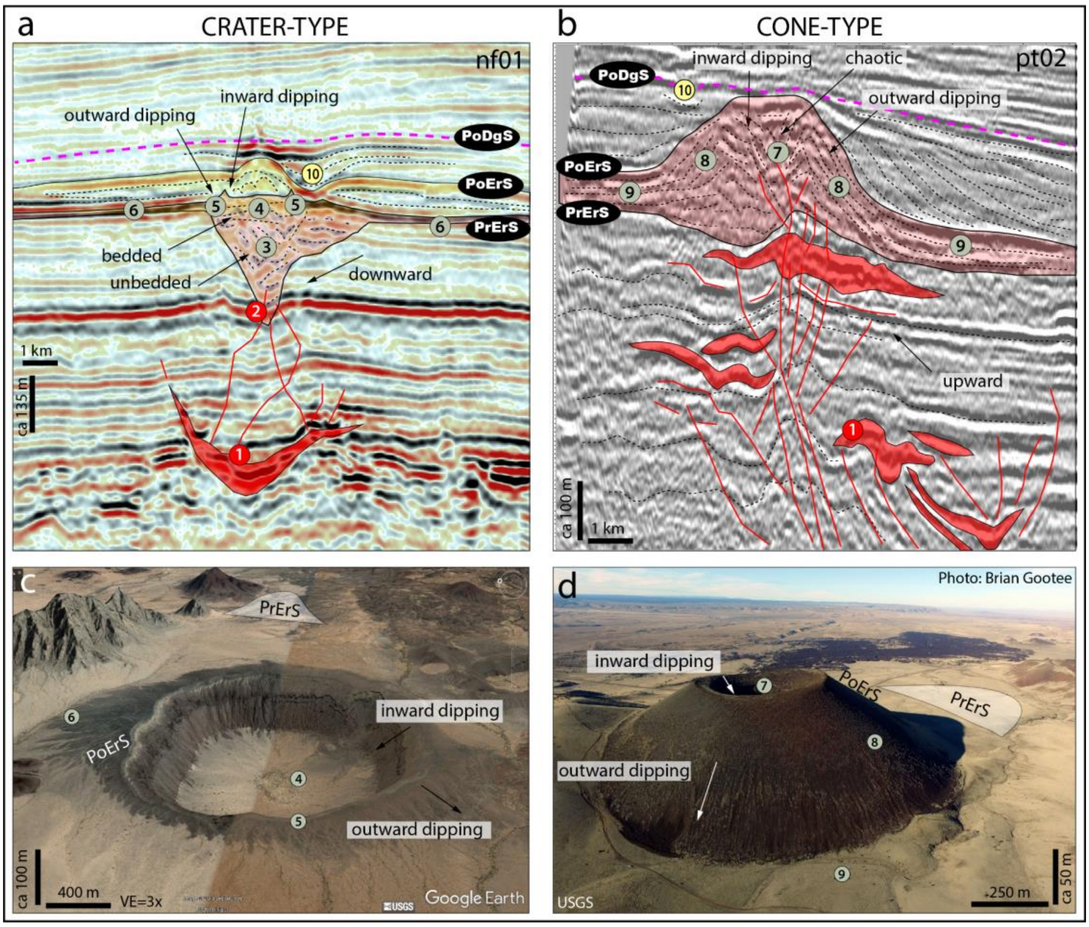

Figure 13: (a and b) shows a 2D seismic section of both crater-and a cone-type volcanoes. (c and d) show analogue crater-and a cone-type morphologies in subaerial monogenetic volcanoes. The crater-type shown in (c) is the maar-diatreme volcano McDougal Crater, in the USA. The cone-type example is the scoria cone SP Crater (USA). Note the geometric similarity between the seismic images and the examples of modern volcanoes, such as the presence of a crater zone with layers inward-dipping, and peripheral flanks with layers outward-dipping. Number in red circles are syn-intrusive bodies, in green are syn-eruptive deposits, and in yellow are post-eruptive deposits. Numbers are: (1) intrusions, (2) root zone, (3) unbedded lower diatreme, (4) bedded upper diatreme, (5) tephra ring, (6) ring plain, (7) central crater, (8) tephra flank, (9) cone apron, (10) canyons. The complete seismic architecture of these volcanoes is shown in Bischoff et al. (2019b).

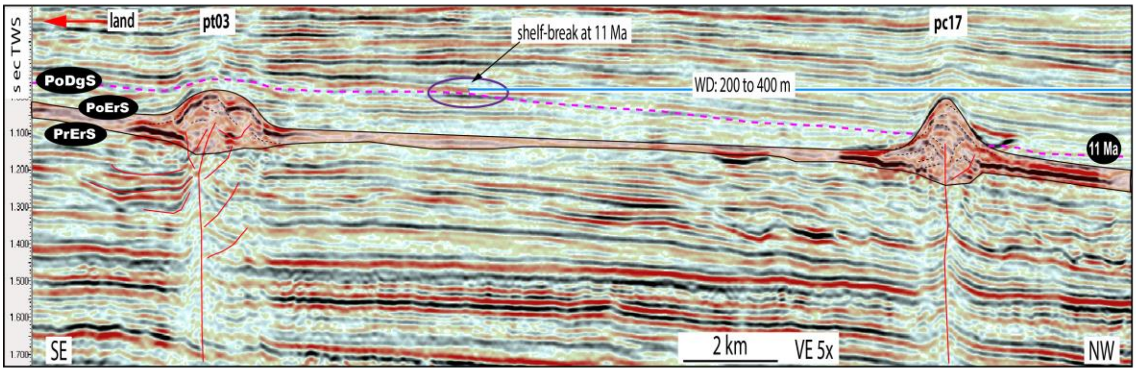

Figure 14: Morphology of the volcanoes pt03 and pc17. Note the mound-shaped morphology of pt03 in contrast to the cone-shaped morphology of pc17. WD and blue line show an interpreted bathymetric depth at ca 11 Ma. Pt03 was likely exposed to the sea-level at 11 Ma and had its form altered by erosional processes, while pc17 was below sea-level and remains well preserved.

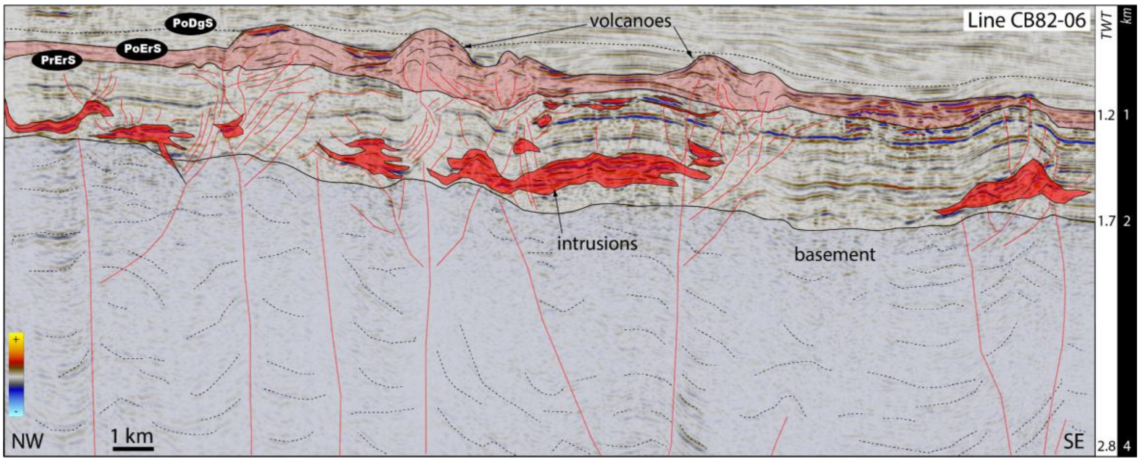

Figure 15: 2D dip section showing the shallow plumbing systems and some of the eruptive vents of the MVF. Note the relationship between the location of intrusive bodies, overlying deformed host strata, and eruptive vents. Below the top of the basement horizon, seismic signal is scattered, and loss of reflectivity produce low quality seismic facies. However, it is still possible to roughly map the location of MVF magmatic conduits based on geometric aspect of internal fabric of the basement.

Acknowledgments

We would like to thanks IHS Markit and Schlumberger for providing academic licence to use the Kingdom and Petrel software. We are grateful to the New Zealand Petroleum and Minerals and the Ministry of Business, Innovation and Employment of New Zealand for providing the dataset and funding for this study. Thanks for the constructive review of Simon Holford, Sverre Planke and Judith Fierstein, and for Te Maire Tau from Ngāi Tahu Research Centre for guidance to select an appropriate name for the Maahunui Volcanic Field.

References

Aarnes I, Planke S, Trulsvik M, Svensen H (2015) Contact metamorphism and thermogenic gas generation in the Vøring and Møre basins, offshore Norway, during the Paleocene-Eocene thermal maximum. J Geol Soc 172: 588-598

Abdelmalak MM, Planke S, Faleide JI, Jerram DA, Zastrozhnov D, Eide S, Myklebust R (2016) The development of volcanic sequences at rifted margins: New insights from the structure and morphology of the Vøring Escarpment, mid-Norwegian Margin: J Geophys Res Sol Earth 121: 5212–5236. doi: 10.1002/2015JB012788.

Agirrezabala L, Sarrionandia F, Carracedo M (2017) Diatreme-forming volcanism in a deep-water faulted basin margin: Lower Cretaceous outcrops from the Basque-Cantabrian Basin, western Pyrenees. J Volcanol Geotherm Res. https://doi.org/10.1016/j.jvolgeores.2017.03.019

Alvarenga R, Iacopini D, Kuchle J, Scherer C, Goldberg, K (2016) Seismic characteristics and distribution of hydrothermal vent complexes in the Cretaceous offshore rift section of the Campos Basin, offshore Brazil. Mar Pet Geol 74 10.1016/j.marpetgeo.2016.03.030.

Angkasa SS, Jerram DA, Millett JM, Svensen HH, Planke S, Taylor RA, Schofield N, Howell J (2017) “Mafic intrusions, hydrothermal venting, and the basalt-sediment transition: Linking onshore and offshore examples from the North Atlantic igneous province”, Interpretation 5 (3), SK83-SK101.

Ballance PF (1993) The New Zealand Neogene forearc basins. In Ballance PF (eds) South Pacific Sedimentary Basins, Sedimentary Basins of the World 2. Elsevier Science, Amsterdam pp 177–193

Barrier, A., 2019. Tectonics, Sedimentation and Magmatism of the Canterbury Basin, New Zealand. Ph.D. Thesis, Canterbury University, New Zealand.

Barrier A, Nicol A, Bischoff AP (2017) Volcanism Occurrences in the Canterbury Basin, New Zealand and Implication for Petroleum Exploration. In AAPG GTW Influence of Volcanism and Associated Magmatic Processes on Petroleum Systems. Conference, Oamaru New Zealand.

Barrier A, Bischoff AP, Nicol A, Browne GH, Bassett K (in prep.) Identification and morphology of buried volcanoes from the Canterbury Basin, New Zealand.

Batt GE, Baldwin SL, Cottam MA, Fitzgerald PG, Brandon MT, Spell TL (2004) Cenozoic plate boundary evolution in the South Island of New Zealand: New thermochronological constraints: Tectonics: doi:10.1029/2003TC001527.

Bischoff AP, Nicol A, Beggs M (2017) Stratigraphy of architectural elements in a buried volcanic system and implications for hydrocarbon exploration: Interpretation. https://doi.org/10.1190/INT-2016-0201.1

Bischoff AP (2019) Architectural Elements of Buried Volcanic Systems and Their Impact on Geoenergy Resources. Ph.D. Thesis, Canterbury University, New Zealand. Pre-print, pp 226. 10.13140/RG.2.2.21440.58886

Bischoff AP, Rossetti M, Nicol A, Kennedy B (2019a) Identification and Characterization of a Buried Volcanic Field Using Seismic Reflection and Borehole Data. Online pre-print in EarthArXiv. Submitted to the Bulletin of Volcanology. 10.31223/osf.io/e64fh

Bischoff AP, Nicol A, Cole J, Gravley D (2019b) Stratigraphy of Architectural Elements of a Buried Monogenetic Volcanic System and Implications for Geoenergy Exploration. Online pre-print in EarthArXiv. Submitted to the Open Geosci. 10.31223/osf.io/h9zuq

Blanke SJ (2010) "Saucer Sills" of the Offshore Canterbury Basin: GNS Publication. https://doi.org:10.1177/0094306114545742f

Clague D, Batiza R, Head JW, Davis A (2000a) Pyroclastic and Hydroclastic Deposits on Loihi Seamount, Hawaii, in Explosive Subaqueous Volcanism, edited by J.D.L. White, J.L. Smellie, and D.A. Clague, American Geophysical Union, Washington D.C., 200. Bull Volcanol https://doi.org/10.1029/140GM05

Clague DA, Moore JG, Reynolds JR (2000b) Formation of Submarine Flat-Topped Volcanic Cones in Hawai'i. In: Explosive Subaqueous Volcanism, edited by J.D.L. White, J.L. Smellie, and D.A. Clague, American Geophysical Union, Washington D.C., 200. Bull Volcanol

Carlson JR, Grant-Mackie JA, Rodgers KA (1980) Stratigraphy and sedimentology of the coalgate area, Canterbury, New Zealand: New Zeal J Geol Geop. https://doi.org/10.1080/00288306.1980.10424205

Cas RAF, Landis CA, Fordyce RE (1989) A monogenetic, Surtla-type, Surtseyan volcano from the Eocene-Oligocene Waiareka-Deborah volcanics, Otago, New Zealand: A model: Bull Volcanol 51 (4): 281-298.

Cas RA, Wright FJV (1993) Volcanic Successions: Modern and Ancient - A Geological Approach to Processes, Products and Successions. Chapman and Hall, UK. https://doi.org:10.1007/978-0-412-44640-5

Cas RA, Giordano FG (2014) Submarine volcanism: A review of the constraints, processes and products, and relevance to the Cabo de Gata volcanic succession. https://doi.org:10.3301/IJG.2014.46

Cas RAF, Simmons JM (2018) Why Deep-Water Eruptions Are So Different From Subaerial Eruptions. Front Earth Sci 6: 198 doi:10.3389/feart.2018.00198.

Catuneanu O (2006) Principles of Sequence Stratigraphy. Changes, 375. https://doi.org:10.5860/CHOICE.44-4462

Coombs DS, White AJR, Hamilton D, Couper RA (1960) Age relations of the Dunedin volcanic complex and some paleogeographic implications—Part II: New Zeal J Geol Geop. https://doi.org:10.1080/00288306.1960.10420145

Coombs DS, Cas RA, Kawachi Y, Landis CA, McDonough WF, Reay A (1986) Cenozoic volcanism in north, east and central Otago. In: Smith IEM (ed) Late Cenozoic Volcanism in New Zealand. R Soc New Zeal Bull 23: 278-312

Deardorff ND, Cashman KV, Chadwick WW (2011) Observations of eruptive plume dynamics and pyroclastic deposits from submarine explosive eruptions at NW Rota-1, Mariana arc. J Volcanol Geotherm Res. https://doi.org/10.1016/j.jvolgeores.2011.01.003

Field BD, Browne GH, Davy BW, Herzer RH, Hoskins RH, Raine JI, Wilson GJ, Sewell RJ, Smale D, Watters WA (1989) Cretaceous and Cenozoic sedimentary basins and geological evolution of the Canterbury region, South Island, New

Zealand. Lower Hutt: New Zealand Geological Survey. New Zealand Geological Survey Basin Studies 2: 94.

Finn CA, Müller RD, Panter KS (2005) A Cenozoic diffuse alkaline magmatic province (DAMP) in the southwest Pacific without rift or plume origin. Geochem Geophys Geosy. https://doi.org/10.1029/2004GC000723

Fornaciai A, Favalli M, Karátson D, Tarquini S, Boschi E (2012) Morphometry of scoria cones, and their relation to geodynamic setting: A DEM-based analysis. J Volcanol Geotherm Res. https://doi.org/10.1016/j.jvolgeores.2011.12.012

Galland O, Bertelsen HS, Eide CH, Guldstrand F, Haug ØT, Héctor, Leanza A, Mair K, Palma O, Planke S, Rabbel O, Rogers B, Schmiedel T, Souche A, Spacapan JB (2018) Storage and transport of magma in the layered crust-Formation of sills and related float-lying intrusions. In: Burchardt S (eds) Volcanic and Igneous Plumbing Systems. Elsevier, pp. 111-136

Hansen DM, Cartwright J (2006) Saucer-Shaped Sill with Lobate Morphology Revealed by 3D Seismic Data: Implications for Resolving a Shallow-Level Sill Emplacement Mechanism. J Geol Soc 163 (3): 509–23. https://doi.org/10.1144/0016-764905-073

Hawkes PW, Mound DD (1984) BP Shell Todd (Canterbury) Services Limited, Clipper-1 Geological Completion Report PR1036.

Head JW, Wilson L (2003) Deep submarine pyroclastic eruptions: theory and predicted landforms and deposits. J Volcanol Geotherm Res 121 (3): 155–193. https://doi.org/10.1016/S0377-0273(02)00425-0

Herzer RH (1995) Seismic Stratigraphy of a Buried Volcanic Arc, Northland, New Zealand and Implications for Neogene Subduction. Mar Pet Geol 12 (5): 511–31. https://doi.org/10.1016/0264-8172(95)91506-K.

Holford SP, Schofield N, MacDonald JD, Duddy IR, Green PF (2012) Seismic Analysis of Igneous Systems in Sedimentary Basins and Their Impacts on Hydrocarbon Prospectivity: Examples from the Southern Australian Margin. APPEA Journal, 52: 229–252.

Holford S, Schofield N, Reynolds P (2017) Subsurface fluid flow focused by buried volcanoes in sedimentary basins: Evidence from 3D seismic data, Bass Basin, offshore southeastern Australia: 39-50. doi:10.1190/INT-2016-0205.1.

Hunt D, Tucker ME (1992) Stranded parasequences and the forced regressive wedge systems tract: deposition during base-level fall: Sediment Geol 81: 1–9. https://doi.org/10.1016/0037-0738(92)90052-S

Infante-Paez L, Marfurt KJ (2017) Seismic expression and geomorphology of igneous bodies: A Taranaki Basin, New Zealand, case study: Interpretation, 5, no. 3, p. SK121-SK140, https://doi.org/10.1190/INT-2016-0244.1

Jackson CAL (2012) Seismic reflection imaging and controls on the preservation of ancient sill-fed magmatic vents. J Geol Soc. https://doi.org/10.1144/0016-76492011-147

Kamp PJJ, Green PF, Tippett JM (1992) Tectonic architecture of the mountain front-foreland basin transition, South Island, New Zealand, assessed by fission track analysis. Tectonics. https://doi.org/10.1029/91TC02362

Kaulfuss U, Németh K, White J (2012) Field Guide Miocene subaerial to subaqueous monogenetic volcanism in Otago, New Zealand.

Klarner S, Klarner O (2012) Identification of Paleo-Volcanic Rocks on Seismic Data, Updates in Volcanology. A Comprehensive Approach to the Volcanological Problems, 181–206, Prof. Francesco Stoppa (eds.), In: Tech, DOI: 10.5772/24943.

Kereszturi G, Németh C (2013) Monogenetic Basaltic Volcanoes: Genetic Classification, Growth, Geomorphology and Degradation: Updates in Volcanology - New Advances in Understanding Volcanic Systems, https://doi.org/10.5772/51387

Laird MG, Bradshaw JD (2004) The Break-up of a Long-term Relationship: the Cretaceous Separation of New Zealand from Gondwana. Gondwana Res 7: 273-286.

Lu H, Fulthorpe S, Mann P (2003) Three-dimensional architecture of shelf-building sediment drifts in the offshore Canterbury Basin, New Zealand. Mar Geol 193: 19-47. 10.1016/S0025-3227(02)00612-6.

Lu H, Fulthorpe CS, Mann P, Kominz MA (2005) Miocene-Recent tectonic and climatic controls on sediment supply and sequence stratigraphy: Canterbury basin, New Zealand: Basin Res 17: 311–328. https://doi.org/10.5772/5138710.1111/j.1365-2117.2005.00266.x

Lorenz V (1985) Maars and diatremes of phreatomagmatic origin, a review. Transactions of the Geological Society of South Africa 88: 459-470.

Marfurt K (2018) Seismic Attributes as the Framework for Data Integration Throughout the Oilfield Life Cycle: Society of Exploration Geophysicists pp 508. https://doi.org/10.1190/1.9781560803522

McLean CE, Schofield N, Brown DJ, Jolley DW, Reid A (2017) 3D seismic imaging of the shallow plumbing system beneath the Ben Nevis Monogenetic Volcanic Field: Faroe–Shetland Basin: J Geol Soc. https://doi.org/10.1144/jgs2016-118

Magee C, Murray H, Christopher JAL, Stephen JM (2019) Burial-Related Compaction Modifies Intrusion-Induced Forced Folds: Implications for Reconciling Roof Uplift Mechanisms Using Seismic Reflection Data. Front Earth Sci. doi:10.3389/feart.2019.00037

Mitchum RM, Vail PR (1977) Seismic Stratigraphy and Global Changes of Sea Level, Part 7 : Seismic Stratigraphic Interpretation Procedure. Seismic Stratigraphy: Applications to Hydrocarbon Exploration. AAPG Memoir 26 Memoir 26: 135–43.

Milne AD (1975) Well completion report Resolution, for BP, Shell, Todd Canterbury Service Limited. New Zealand Geological Survey Open-file Petroleum Report No. 648.

Morley C (2018) 3D seismic imaging of the plumbing system of the Kora volcano, Taranaki Basin, New Zealand: The influences of syn-rift structure on shallow igneous intrusion architecture: Geosphere 2018. doi.org/10.1130/GES01645.1.

Mortimer N (2004) New Zealand's Geological Foundations: Gondwana Research, v. 7, no. 1, p. 261-272.

Németh K, White JDL (2003) Reconstructing eruption processes of a Miocene monogenetic volcanic field from vent remnants: Waipiata Volcanic Field, South Island, New Zealand. J Volcanol Geotherm Res doi:10.1016/S0377-0273(03)00042-8.

Németh K (2010) Monogenetic volcanic fields; origin, sedimentary record, and relationship with polygenetic volcanism: Special Paper Geological Society of America, https://doi.org/10.1130/2010.2470(04)

Németh K, Kereszturi G (2015) Monogenetic volcanism: personal views and discussion. Int J Earth Sci (Geol Rundsch) 104: 2131. https://doi.org/10.1007/s00531-015-1243-6

Oliveira L, Gama R, Pereira E (2017). Seismic characteristics of the onshore Abrolhos magmatism, East-Brazilian continental margin. Mar Pet Geol. 10.1016/j.marpetgeo.2017.10.016.

Penna R, Araujo S, Sansonowski R, Oliveira L, Rosseto J, Geisslinger A, Matos M (2018) Igneous rock characterization through reprocessing, FWI imaging, and elastic inversion of a legacy seismic dataset in Brazilian Pre-Salt Province: pp 3277-3281. 10.1190/segam2018-2996032.1. https://doi.org/10.1190/segam2018-2996032.1

Planke S, Rasmussen T, Rey SS, Myklebust R (2005) Seismic characteristics and distribution of volcanic intrusions and hydrothermal vent complexes in the Vøring and Møre basins, in Petroleum Geology: North-West Europe and Global Perspectives – Proceedings of the 6th Petroleum Geology Conference: doi:10.1144/0060833.

Planke S, Alvestad E, Eldholm O (1999) Seismic Characteristics of Basaltic Extrusive and Intrusive Rocks. The Leading Edge 18: 342. https://doi.org/10.1190/1.1438289

Planke S, Symonds PA, Alvestad E, Skogseid J (2000) Seismic Volcanostratigraphy of Large-Volume Basaltic Extrusive Complexes on Rifted Margins. J Geophys Res 105 (B8): 19335. https://doi.org/10.1029/1999JB900005

Planke S, Millett JM, Maharjan D, Jerram DA, Abdelmalak MM, Groth A, Hoffmann J, Berndt C, Myklebust R (2017) Igneous seismic geomorphology of buried lava fields and coastal escarpments on the Vøring volcanic rifted margin: Interpretation. https://doi.org/10.1190/INT-2016-0164.1

Planke S, Rabbel O, Galland O, Millett J, Manton B, Jerram D, Palma O, Spacapan J (2018) Seismic Imaging and Petroleum Implications of Igneous Intrusions in Sedimentary Basins Constrained by Outocrop Analogues and Seismic Data from the Neuquen Basin and the NE Atlantic.

Reynolds P, Schofield N, Brown RJ, Holford SP (2016) The architecture of submarine monogenetic volcanoes - insights from 3D seismic data: Basin Res 30: 437–451. https://doi.org/10.1111/bre.12230

Reynolds P, Holford S, Schofield N, Ross A (2017) Three-Dimensional Seismic Imaging of Ancient Submarine Lava Flows: An Example From the Southern Australian Margin. Geochem Geophys Geosys https://doi.org/1002/2017GC007178

Sahoo TR, Kroeger KF, Thrasher G, Munday S, Mingard H, Cozens N, Hill M (2015) Facies Distribution and Impact on Petroleum Migration in the Canterbury Basin, New Zealand: In: Eastern Australian Basins Symposium 2015: Publication of Proceedings. Petroleum Exploration Society of Australia, Perth, WA, p. 187-202.

Silva SD, Lindsay JM (2015) Primary Volcanic Landforms. In: The Encyclopedia of Volcanoes. https://doi.org/10.1016/B978-0-12-385938-9.00015-8

Schofield N, Heaton L, Holford SP, Archer SG, Jackson CAL, Jolley DW (2012) Seismic imaging of “broken bridges”: linking seismic to outcrop-scale investigations of intrusive magma lobes: J Geol Soc doi:10.1144/0016-76492011-150.

Schofield N, Jerram DA, Holford S, Stuart A, Niall M, Hartley A, Howell J, David M, Green P, Hutton D, Stevenson C (2016) Sills in sedimentary basin and petroleum systems: In Németh K (ed) The Series Advances in Volcanology, pp 1–22.

Sewell RJ (1988) Late Miocene volcanic stratigraphy of central Banks Peninsula, Canterbury, New Zealand pp. 41–64. https://doi.org/10.1080/00288306.1988.10417809

Schiøler P, Raine JI, Griffin A, Hollis CJ, Kulhanek DK, Morgans HEG, Roncaglia L, Strong CP, Uruski C (2011) Revised biostratigraphy and well correlation, Canterbury Basin, New Zealand. GNS Science Consultancy Report 2011/12. 142 p.

Strogen DP, Seebeck H, Nicol A, King PR (2017) Two-phase Cretaceous–Paleocene rifting in the Taranaki Basin region, New Zealand; implications for Gondwana break-up: Journal of the Geological Society, https://doi.org/10.1144/jgs2016-160

Suggate RP, Stevens GR, Te Punga MT (1978) The geology of New Zealand. Govt Printer, Wellington.

Svensen HH, Planke S, Malthe-Sørenssen A, Jamtveit B, Myklebust R, Eidem T, Rey S S (2004) Release of methane from a volcanic basin as a mechanism for initial Eocene global warming. Nature, 429, 542-545.

Timm C, Hoernle K, Werner R, Hauff F, van den Bogaard P, White J, Mortimer N, Garbe-Schönberg D (2010) Temporal and geochemical evolution of the Cenozoic intraplate volcanism of Zealandia. https://doi.org/10.1016/j.earscirev.2009.10.002

White JDL (2000) Subaqueous eruption-fed density currents and their deposits: Precambrian Res 101: 87–109. https://doi.org/10.1016/S0301-9268(99)00096-0

White JDL, Ross PS (2011) Maar-diatreme volcanoes: A review. https://doi.org/10.1016/j.jvolgeores.2011.01.010

White JDL, Schipper CI, Kano K (2015a) Submarine Explosive Eruptions. In: The Encyclopedia of Volcanoes. https://doi.org/10.1016/B978-0-12-385938-9.00031-6

White JDL, McPhie J, Soule SA (2015b) Submarine Lavas and Hyaloclastite. In: The Encyclopedia of Volcanoes. https://doi.org/10.1016/B978-0-12-385938-9.00019-5

White JDL, Valentine GA (2016) Magmatic versus phreatomagmatic fragmentation: Absence of evidence is not evidence of absence. Geosphere 12: 1478–1488. https://doi.org/10.1130/GES01337.1

Wright IC, Worthington TJ, Gamble JA (2006) New multibeam mapping and geochemistry of the 30°-35° S sector, and overview, of southern Kermadec arc volcanism. J Volcanol Geotherm Res. https://doi.org/10.1016/j.jvolgeores.2005.03.021

Zimanowski B, Büttner R, Lorenz V, Häfele HG (1997) Fragmentation of basaltic melt in the course of explosive volcanism. J Geophys Res Sol Earth. doi:10.1029/96JB02935

Zimanowski B, Büttner R (2003) Phreatomagmatic explosions in subaqueous volcanism. In: Geophysical Monograph Series: https://doi.org/10.1029/140GM03